DEVELOPMENT OF NOVEL POLY(VINY ALCOHOL)/GRAPHENE NANOCOMPOSITES

A THESIS SUBMITTED TO
THE GRADUATE SCHOOL OF NATURAL AND APPLIED SCIENCES

OF
ATILIM UNIVERSITY

BY
MELIKE GOZUTOK

THE DEPARTMENT OF METALLURGICAL AND MATERIALS ENGINEERING

JULY 2017

Approval of the Graduate School of Natural and Applied Sciences, Atılım University.

_____

Prof. Dr. Ali Kara

I certify that this thesis satisfies all the requirements as a thesis for the degree of Master of Science.

_____

Prof. Dr. Naci SEVINC
Head of Department

This is to certify that we have read the thesis "DEVELOPMENT OF NOVEL POLY(VINYL ALCOHOL)/GRAPHENE NANOCOMPOSITES" submitted by "Melike Gozutok" and that in our opinion it is fully adequate, in scope and quality, as a thesis for the degree of Master of Science.

_____

Assoc. Prof. Dr. Hilal TURKOGLU SASMAZEL
Supervisor

Examining Committee Members

Assoc. Prof. Dr. Hilal Turkoglu Sasmazel _____

Assoc. Prof. Dr. Halil Murat Aydin _____

Assist. Prof. Dr. Kemal Davut _____

Date: 10.07.2017

I declare and guarantee that all data, knowledge and information in this document has been obtained, processed and presented in accordance with academic rules and ethical conduct. Based on these rules and conduct, I have fully cited and referenced all material and results that are not original to this work.

Name, Last name: Melike, GOZUTOK

Signature:

ABSTRACT

DEVELOPMENT OF NOVEL POLY(VINYL ALCOHOL)/GRAPHENE NANOCOMPOSITES

Gozutok, Melike

M.S., Metallurgical and Materials Engineering Department

Supervisor: Assoc. Prof. Dr. Hilal Turkoglu Sasmazel

July 2017, 75 pages

The aim of this study was to develop nanocomposites by electrospinning with poly (vinyl alcohol) (PVA) and the forms of graphene, reduced graphene oxide (rGO) and Chemical Vapor Deposited (CVD)-grown monolayer graphene, in order to use them in possible applications such as packaging, electrical, thermal and tissue engineering. For this purpose, 2 major different approaches were utilized. First approach was electrospinning of PVA and rGO blend with different rGO contents (0.5 and 1 wt %), while the second approach was electrospinning of PVA solution onto a CVD-grown monolayer graphene. After crosslinking of the nanocomposites, the common characterizations were done by thickness and contact angle (CA) measurements; scanning electron microscopy (SEM), mechanical property and thermogravimetric (TGA) analyses; PBS absorption and shrinkage tests, in vitro degradation and electrical conductivity measurements. Besides, chemical examinations were done via Fourier Transmission Infrared Spectroscopy (FTIR) analyses, crystallinity observations were done with X-ray Diffraction (XRD) and water vapor transmission rate (WVTR) analyses for PVA/rGO nanocomposites while optical microscopy and Raman analyses were performed for PVA electrospun CVD-grown monolayer graphene nanocomposites. The highest fiber diameter belonged to electrospun PVA+0.5 wt% rGO (~388 nm) nanocomposites whereas the lowest fiber diameter was measured for the electrospun PVA mats (~340 nm). On the other hand, the highest electrical conductivity was recorded as ~11 $\mu S.cm^{-1}$ for electrospun PVA+1.0 wt% rGO. Additionally cell-material interactions were observed with MG-63

osteosarcoma cell-line. At the end, it was suggested that electrospun PVA+1.0 wt% rGO nanocomposites were highly suitable candidates to be used in possible applications.

Keywords: Electrospun PVA, reduced graphene oxide (rGO), CVD-grown monolayer graphene, MG-63 cell culture, nanocomposites, electrical and thermal applications.

ÖZ

POLİ(VİNİL ALKOL)/GRAFEN NANOKOMPOZİTLERİN GELİŞTİRİLMESİ

Gözütok, Melike
Yüksek Lisans, Metalurji ve Malzeme Mühendisliği Bölümü
Tez Danışmanı: Doç. Dr. Hilal Türkoğlu Şaşmazel
Temmuz 2017, 69 sayfa

Çalışmanın amacı, polivinil alkol (PVA) ve grafenin formlarından indirgenmiş grafen oksit (rGO) ve kimyasal buharla biriktirilmiş (CVD) tek tabaka grafenin elektroeğirilmesiyle olası uygulamalarda (paketleme, elektriksel, termal ve doku mühendisliği) kullanılmak üzere yeni nanokompozitlerin elde edilmesidir. Bu amaç doğrultusunda iki farklı yöntem kullanılmıştır. Bunlardan ilki satın alınan PVA ve farklı yüzdelerdeki (ağırlıkça % 0.5 ve 1) rGO karışımının elektroeğirilmesiyken, diğeri PVA'nın CVD tek tabaka grafene elektroeğirilmesidir. Elde edilen nanokompozitlerin UV ışını ile çapraz bağlanmasının ardından, her iki tip malzemenin karakterizasyon özelliklerinin belirlenmesi; kalınlık, iletkenlik ve yüzey temas açısı (CA) ölçümleri, taramalı elektron mikroskobu (SEM), termogravimetrik (TGA) ve su, mekanik ve degredasyon (bozunma) testleri ve PBS şişme ve büzüşme davranış tayinleri ile yapılmıştır. Bunun yanı sıra rGO/PVA nanokompozitlerinin kimyasal kompozisyonları Fourier Dönüşümlü Kızılötesi Spektrofotometre (FTIR), kristal yapıdaki değişim X-ışını Kırınım (XRD) ile incelenmiş ek olarak su buharı geçirgenlik analizleri (WVTR) yapılmış; PVA elektroğrilmiş CVD tek tabaka grafen nanokompozitleri için ayrıca optik mikroskop ve Raman analizleri yapılmıştır. Bu analizler sonucunda, en yüksek fiber çapı ~340 nm ile elektroeğirilmiş %0.5 rGO+PVA nanokompozitleri için ölçülürken, en yüksek elektrik iletkenlik değeri elektroeğirilmiş % 1.0 rGO+PVA nanokompozitleri için ~11 $\mu S.cm^{-1}$ olarak

bulunmuştur. Bu analizlere ek olarak, hazırlanan nanokompozitlerin hücre-materyal etkileşimleri MG-63 hücre hattı kullanılarak gerçekleştirilmiştir. Tüm bu analizlerin sonucunda % 1.0 rGO+PVA tipi nanokompozitin olası uygulamalarda (paketleme, elektriksel, termal ve doku mühendisliği) kullanmak üzere oldukça uygun ve yararlı bir malzeme olduğu anlaşılmıştır.

Anahtar kelimeler: Elektroeğirilmiş PVA, indirgenmiş grafen oksit, CVD tek tabaka grafen, MG-63 hücre kültürü, nanokompozit, elektriksel ve termal uygulamalar.

To my beloved parents who always encourage me to learn…

ACKNOWLEDGEMENTS

Foremost, I would like to express my sincere gratitude to my advisor Assoc. Prof. Dr. Hilal Sasmazel for her continuous support of my master study and research, for her patience, motivation, enthusiasm, encouragement and immense knowledge. Her guidance helped me in all the time of research and writing of this thesis. Besides, she consistently allowed this paper to be my own work, but steered me in the right direction whenever she thought I needed it. She believed in me more than I believed in myself. I could not have imagined having a better advisor and mentor for my master study.

I would like to thank the rest of my thesis committee; Assoc. Prof. Dr. Halil Murat Aydın and Assist. Prof. Dr. Kemal Davut, for their support.

I would like to thank Ozan Ozkan, PhD, for his advices and supports. I am so thankful to him because the door to his office was always open whenever I ran into a trouble spot or had a question about my research or writing.

I would like to thank Assoc. Prof. Dr. Halil Murat Aydın for supplying MG-63 Osteosarcoma cell line to our group for my thesis.

I would like to thank Assist. Prof.Dr. Kemal Davut and Ebru Arslan for their support in the cell culture SEM analyses of my thesis.

Finally, I must express my very profound gratitude to my family and to my friends, especially to Ozlem Agac, for providing me with unfailing support and continuous encouragement throughout my years of study and through the process of researching and writing this thesis. This accomplishment would not have been possible without them.

TABLE OF CONTENTS

ABSTRACT iv
ÖZ vi
ACKNOWLEDGEMENTS ix
TABLE OF CONTENTS x
LIST OF TABLES xiii
LIST OF ABBREVIATIONS xvi
CHAPTER 1 1
Introduction 1
CHAPTER 2 4
Literature Survey 4
2.1. Nanocomposites 4
2.1.2. Types of Nanocomposites 5
2.1.2.1. Metal-Matrix Nanocomposites 5
2.1.2.2. Polymer-Matrix Nanocomposites 6
2.1.2.3. Ceramic-Matrix Nanocomposites 7
2.1.3. Applications of the Nanocomposites 7
2.1.3.1. Aerospace Applications 7
2.1.3.2. Food Packaging 8
2.1.3.3. Electrical Applications 8
2.1.3.4. Tissue Engineering Applications 9
2.2. Electrospinning Process 11
2.2.1. Parameters Affecting the Process 11
2.2.1.1. Solution Parameters 12
2.2.1.2. Process Parameters 13
2.2.1.3. Ambient Parameters 14
2.2.2. Types of Electrospinning Setups 14
2.2.3. Applications of Electrospinning 16
2.3. Poly(vinyl alcohol) 16
2.4. Graphene 18
2.4.1. Graphene Oxide (GO) 19
2.4.1.1. Reduced Graphene Oxide (rGO) 20

2.4.2. CVD-Grown Graphene 21
CHAPTER 3 23
Experimental Study 23
3.1. Materials 23
3.2. Preparation of the Nanocomposites 23
3.2.1. PVA+rGO Nanocomposites 23
3.2.1.1. Preparation of the Solutions 23
3.2.1.2. Optimization and Determination of Electrospinning Process 24
3.2.2. PVA Electrospun CVD-Grown Monolayer Graphene Nanocomposites 25
3.2.2.1. Synthesis of Monolayer Graphene 25
3.2.2.2. Preparation of PVA Solution 26
3.2.2.3. Determination of Electrospinning Process 26
3.3. Production of the Nanocomposites 26
3.3.1. Crosslinking of the Nanocomposites 27
3.4. Characterizations 27
3.4.1. Thickness Measurements 27
3.4.2. Contact Angle (CA) Measurements 27
3.4.3. Optical Microscopy Analyses 28
3.4.4. Scanning Electron Microscopy (SEM) Analyses 28
3.4.5. Mechanical Properties 28
3.4.6. Attenuated Total Reflection Fourier Transform Infrared Spectroscopy (ATR-FTIR) Analyses 28
3.4.7. Thermogravimetric (TGA) Analyses 28
3.4.8. X-Ray Diffraction (XRD) Analyses 29
3.4.9. Raman Analyses 29
3.4.10. PBS Absorption and Shrinkage Tests 29
3.4.11. In Vitro Degradation 30
3.4.12. Water Vapor Transmission Rate (WVTR) 30
3.4.13. Electrical Conductivity Measurements 30
3.5. Cell Culture Studies 31
3.5.1. MTT Assay 31
3.5.2. ALP Activity 32
3.5.3. Alizarin Red Staining 32
3.5.4. Fluorescence Microscopy Analyses 32
3.5.5. Observation with SEM 33
CHAPTER 4 34

Results and Discussions 34
4.1. Production of the Nanocomposites 34
4.1.1. Crosslinking of the Nanocomposites 34
4.2. Characterizations 34
4.2.1. Thickness, the Average Fiber Diameter, the Average Inter-Fiber Pore Size and Porosity (%) Values 34
4.2.2. Contact Angle (CA) (°) Measurements 36
4.2.3. Optical Microscopy Analyses 37
4.2.4. Scanning Electron Microscope (SEM) Analyses 38
4.2.5. Mechanical Properties 40
4.2.6. ATR-FTIR Analyses 42
4.2.7. TGA Analyses 43
4.2.8. XRD Analyses 44
4.2.9. Raman Analyses 46
4.2.10. PBS Absorption and Shrinkage Tests 47
4.2.11. In Vitro Degradation 48
4.2.12. WVTR 49
4.2.13. Electrical Conductivity Measurements 50
4.3. Cell Culture Studies 51
4.3.1. MTT Assay 51
4.3.2. ALP Activity 52
4.3.3. Alizarin Red Staining 53
4.3.4. Fluorescence Microscopy Analyses 55
4.3.5. Observations with SEM 56
CHAPTER 5 57
Conclusions 57
REFERENCES 61

LIST OF TABLES

Table 1. Electrospinning process parameters of PVA+0.5 wt% rGO. 24

Table 2. Electrospinning process parameters of PVA+1.0 wt% rGO. 25

Table 3. Properties of the nanocomposites *(p<0.0005)*. 36

Table 4. CA (°) values of the samples. 37

Table 5. Tensile properties of the nanocomposites. 41

Table 6. PBS absorption (%) and shrinkage (%) values of the samples. 48

Table 7. Electrical conductivity of the nanocomposites. 51

LIST OF FIGURES

Figure 1. Vertical electrospinning setup. 15

Figure 2. Horizontal electrospinning setup. 15

Figure 3. Coaxial electrospinning setup with a modified nozzle. One syringe to feed the core and the other to feed the shell solution. 15

Figure 4. Schematic representation of a graphene lattice. 18

Figure 5. Optical microscopy images of CVD-grown monolayer graphene at Cu foil (a) x40, (b) x100; Cu foil only (c) x40, (d) x100. 38

Figure 6. SEM images of electrospun a) PVA fibers, b) PVA+0.5 wt% rGO fibers and c) PVA+1.0 wt% rGO fibers x20000; d) PVA fibers, e) PVA+0.5 wt% rGO fibers and e) PVA+1.0 wt% rGO fibers x50000; f') cross-section of electrospun PVA+1.0 wt% rGO fibers x2500. 39

Figure 7. SEM images of (a) CVD-grown monolayer graphene at Cu foil, (b) Cu foil only, x5000. 40

Figure 8. SEM images of PVA electrospun CVD-grown monolayer graphene nanocomposites (a) x1000, (b) x10000, (c) x20000. 40

Figure 9. FTIR spectra of a) commercial rGO, electrospun b) PVA mats, c) PVA+0.5 wt % rGO and d) PVA+1.0 wt % rGO nanocomposites. 43

Figure 10. TGA curves of nanocomposites. 44

Figure 11. XRD patterns of a) commercial rGO, electrospun b) PVA mats, c) PVA+0.5 wt % rGO and d) PVA+1.0 wt % rGO nanocomposites. 45

Figure 12. The raman spectra of a) electrospun PVA, b) neat CVD-grown monolayer graphene and c) PVA electrospun CVD-grown monolayer graphene. 47

Figure 13. Weight remaining electrospun PVA mats, PVA+0.5 wt % rGO, PVA+1.0 wt % rGO and PVA electrospun CVD-grown monolayer graphene nanocomposites of as a function of degradation time. 49

Figure 14. WVTR of electrospun PVA mats, PVA+0.5 wt % rGO and PVA+1.0 wt % rGO nanocomposites. 50

Figure 15. Absorbance values of the nanocomposites by MTT 52

Figure 16. ALP activity of the MG-63 cells on the nanocomposites (BCIP tablet was used as blank substrate and its value was accepted as 100) 53

Figure 17. Quantification of MG-63 cell mineralization cultured on the nanocomposites.... 54

Figure 18. The color change as a result of Ca^{+2} deposition on a)TCPS, b) electrospun PVA, c) PVA electrospun CVD-grown monolayer graphene, d) PVA+0.5 wt % rGO, e) PVA+1.0 wt % rGO nanocomposites on 7^{th}, 14^{th} and 21^{st} days of cultivation. 54

Figure 19. Flourescence images (by DAPI stain) a) TCPS, b) Electrospun PVA, c) CVD-grown monolayer graphene, d) Electrospun PVA+0.5 wt % rGO e) Electrospun PVA+1.0 wt % rGO nanocomposites, on 7^{th}, 14^{th} and 21^{st} days of cultivation. 55

Figure 20. SEM images of MG-63 cells on/within electrospun PVA on a) 7^{th} day, x500, b) 21^{st} day, x500, c) 21^{st} day, x10000; and electrospun PVA+1.0 wt % rGO nanocomposites d) 7^{th} day, x500 e) 21^{st} day, x500, f) 21^{st} day, x10000. 56

LIST OF ABBREVIATIONS

PVA	-	Poly (vinyl alcohol)
rGO	-	Reduced graphene oxide
TCPS	-	Tissue Culture Polystyrene
CA	-	Contact Angle
SEM	-	Scanning Electron Microscopy
FTIR	-	Fourier Transformation Infrared Spectroscopy
TGA	-	Thermogravimetric Analyses
XRD	-	X-Ray Diffractometer
PBS	-	Phosphate Buffer Saline
BSA	-	Bovine Serum Albumin
DMEM/F12	-	Dulbecco's Modified Eagle Medium
FBS	-	Fetal Bovine Serum

CHAPTER 1

Introduction

Nanocomposites are the advanced materials, with their improved properties (electrical conductivity, thermal, mechanical, lightweight and biological properties), mainly used in nanoengineering, bioengineering, electrical engineering, drug delivery and food engineering [1-4]. In a nanocomposite material, generally the structure is a matrix-filler combination where the fillers can be fibers, particles, or fragments surrounds and binds together as discrete units in the matrix [5]. In the simplest way, nanocomposites are divided into 3 main groups; metal-matrix, polymer-matrix and ceramic-matrix nanocomposites. Among those, polymer-matrix nanocomposites are widely used in ***scaffold-base tissue engineering*** because of the improved biological properties with being non-toxic [6-7]. On the other hand, all types of nanocomposites can be used in ***electrical applications*** due to their improved conductivity, mechanical and thermal properties [8-9].

As the technology is developed, the interest on nanocomposites is increased, and the nanocomposite production processes became easier. One of the easiest and fascinating ways to obtain nanocomposites is electrospinning process which produces nanofibers from variety of precursors which could be polymers, composites, and ceramics. Principally, electrostatic charges make the precursor solution be stretched towards the electrode, and at the same time evaporation of solvent occurs. At the end, desired fibers are collected on the counter electrode [10-11]. By electrospinning, high surface area to volume ratio can be obtained, thus electrospinning is highly preferred for preparation of the nanocomposites. To design biomedical nanocomposites by electrospinning, wide range of natural and synthetic polymers are used such as, cellulose, chitosan, gelatin, collagen, fibrin, poly(vinyl alcohol) (PVA), poly(ethylene glycol) (PEG), poly(caprolactone) (PCL), poly(lactic-co-glycolic acid) (PLGA), and poly(glycerol sebacate) (PGS) [10]. On the other

hand, due to the improved electrical conductivity, graphene and its nanocomposites are being prepared by electrospinning to be served in electrical applications [12-13].

PVA is a synthetic and water-soluble polymer which has a melting point of 230 °C. It is partially crystalline and it has excellent mechanical, thermal and biological properties. For this reason, PVA and its nanocomposites are highly preferred in tissue engineering and electrical applications [14-15].

On the other hand, graphene, which is an allotrope of carbon, is the strongest material ever known [16]. Because of its unique electrical, thermal and mechanical properties, nanocomposites of graphene are frequently used in several applications for both industry and science. Lately, the forms of graphene are produced to use them in the most effective way. Graphene oxide is the most produced form of graphene and they are generally used as flakes. By the oxidization and reduction processes, graphene oxide can be reduced in order to be used in nano-scale applications. The obtained reduced form of graphene oxide is called as 'reduced graphene oxide (rGO)' [17]. rGO is the form of high quality graphene and they are generally used to produce nanocomposites to be applied in many applications such as nanotechnology, biotechnology and electrical applications [17-19].

The other high quality form of graphene is obtained by chemical vapor deposition (CVD) technique. Basically, CVD can be defined as the process of depositing gaseous reactants onto a substrate. Creation of CVD graphene is generally done in two steps, the precursor pyrolysis of a material to form carbon, and the carbon structure formation of graphene by using disassociated carbon atoms. Because of the obtained high quality graphene, CVD grown graphene is commonly used in many applications such as; filtration, electrical applications, sensors, electrodes and catalytic applications, nanoengineering and bioengineering technology [20-21].

Our strategy in this study was to develop nanocomposites by electrospinning with using PVA and the forms of graphene in order for them to be used in possible applications such as packaging, electrical, thermal and tissue engineering applications. Basically, 2 major different approaches were utilized for this purpose. First approach was electrospinning of PVA and rGO blend with different rGO contents (0.5 and 1 wt%), while the second approach was electrospinning of PVA solution onto a CVD-grown monolayer graphene. Optimum solution and process

parameters were decided either with the help of literature or the optimization experiments. Morphology of the obtained fibers was examined with SEM analyses and the wettability of the nanocomposites was decided with CA measurements and thermal behaviors were examined via TGA analyses. The chemical examinations were done via FTIR analyses, crystallinity observations were done with XRD analyses and WVTR analyses were done the for rGO+PVA nanocomposites. Molecular vibrations were observed with Raman spectroscopy and surface properties were examined with optical microscopy for PVA electrospun CVD-grown monolayer graphene nanocomposites. Additionally, thickness measurements, electrical and mechanical property analyses, PBS absorption, in-vitro degradation and WVTR studies were performed for the obtained nanocomposites. Finally, cell-material interactions of the candidate nanocomposites were investigated by in vitro cell culture studies with MG-63 cell line for 21 day-period culture.

CHAPTER 2

Literature Survey

2.1. Nanocomposites

A nanocomposite is a structural matrix to which nanoparticles are added to improve a special property of the material which exhibits unusual property combinations and unique design possibilities [22].

Nanocomposites are the composite materials in which one of the phases has one, two or three dimensions of less than 100 nanometers (nm), or structures having nano-scale repeat distances between the different phases that make up the material [22]. The main reason for adding nanoscale second phase is to create a synergy between the various constituents, such that novel properties capable of meeting or exceeding design expectations can be achieved [23]. The properties of nanocomposites rely on a range of variables, specially the matrix material, that can exhibit nanoscale dimensions, loading, size, degree of dispersion, shape and orientation of the nanoscale second phase and the interactions between the matrix and the second phase.

Nanocomposites differ from conventional composite materials because of the exceptionally high surface to volume ratio of the reinforcing phase and/or its exceptionally high aspect ratio, in mechanical manner. The reinforcing material can be made up of particles (e.g. minerals), sheets (e.g. exfoliated clay stacks) or fibers (e.g. carbon nanotubes or electrospun fibers). The area of the interface between the matrix and reinforcement phase(s) is typically an order of magnitude greater than for conventional composite materials. The matrix material properties are significantly affected in the vicinity of the reinforcement [24]. This large amount of reinforcement surface area means that a relatively small amount of nanoscale reinforcement can have an observable effect on the macroscale properties of the composite. For example, adding carbon nanotubes improves the electrical and thermal conductivity.

Other kinds of nanoparticulates may result in enhanced optical properties, dielectric properties, heat resistance or mechanical properties such as stiffness, strength and resistance to wear and damage. In general, the nano reinforcement is dispersed into the matrix during processing. The percentage by weight, which is called as mass fraction, of the nanoparticulates introduced can remain very low due to the low filler percolation threshold, especially for the most commonly used non-spherical, high aspect ratio fillers (e.g. nanometer-thin platelets, such as clays, or nanometer-diameter cylinders, such as carbon nanotubes). The orientation and arrangement of asymmetric nanoparticles, thermal property mismatch at the interface, interface density per unit volume of nanocomposite, and polydispersity of nanoparticles significantly affect the properties of the nanocomposites [24].

Main advantages of using nanocomposites are,

- Mechanical properties e.g. strength, modulus and dimensional stability,
- Decreased permeability to gases, water and hydrocarbons,
- Thermal stability and heat distortion temperature,
- Flame retardancy and reduced smoke emissions,
- Chemical resistance,
- Surface appearance,
- Electrical conductivity,
- Optical clarity in comparison to conventionally filled polymers.

2.1.2. Types of Nanocomposites

Basically, nanocomposites can be classified into 3 major groups which are metal-matrix, polymer-matrix and chemical-matrix nanocomposites.

2.1.2.1. Metal-Matrix Nanocomposites

Metal matrix nanocomposites (MMNC) are also called as reinforced metal matrix composites and they can be categorized as continuous and non-continuous reinforced materials. In recent years, the attention on metal matrix nanocomposites has increased in various areas of industry because of their special mechanical and

physical properties [25]. Carbon Nanotube Metal Matrix Composites (CNT-MMNC) is one of the most significant types of these nanocomposites, which is an emerging material that is being developed because of taking advantage of the high tensile properties and electrical conductivity of these nanotubes [26]. In addition to carbon nanotubes, boron nitride reinforced metal matrix composites and carbon nitride metal matrix composites are the new developed research areas for metal matrix nanocomposites [27-28]. On the other hand, at elevated temperatures, aluminum based composites have high specific strength and stiffness as well as fatigue, corrosion and wear resistance. Consequently, MMNC's are alternative materials that can be replaced with conventional materials in numerous fields of application such as automotive, aeronautical and aerospace, and in other advanced industries.

2.1.2.2. Polymer-Matrix Nanocomposites

Polymer-matrix nanocomposites (PMNC) can be defined as the nanocomposites consist of a polymer or copolymer that has nanoparticles or nanofillers dispersed in a polymer matrix [29]. The nanoparticulates which are added on the polymer matrix may be different shape, such as platelets, fibers, spheroids, but at least one dimension of those must be in the range of 1–50 nm. As the simplest case, adding nanoparticulates appropriately to a polymer matrix can improve its performance, by simply capitalizing on the nature and properties of the nanoscale filler [30]. Specially, this strategy is very effective for yielding high performance composites, while good dispersion of the filler is achieved and the properties of the nanoscale filler are devoutly different or better than those of the matrix.

Most of the polymeric nanocomposites are used for biomedical applications like tissue engineering, drug delivery, cellular therapies [31-32]. Because of the unique interactions between polymer and nanoparticles, a range of property combinations can be engineered to mimic native tissue structure and its properties. A range of natural and synthetic polymers are used to design polymeric nanocomposites for biomedical applications including starch, alginate, cellulose, chitosan, gelatin, collagen, fibrin, poly(vinyl alcohol) (PVA), poly(ethylene glycol) (PEG), poly(caprolactone) (PCL), poly(lactic-co-glycolic acid) (PLGA), and poly(glycerol sebacate) (PGS) [33-35]. Besides, a range of nanoparticles including ceramic, polymeric, metal oxide and carbon-based nanomaterials are incorporated within polymeric network to obtain desired property combinations.

2.1.2.3. Ceramic-Matrix Nanocomposites

In ceramic-matrix nanocomposites, the main part of the volume is occupied by a ceramic, i.e. a chemical compound from the group of oxides, borides, nitrides, silicates etc. Generally, ceramic-matrix nanocomposites encompass a metal as a second component. Optimally both of these components are finely dispersed in each other to provide the particular nanoscopic properties. Nanocomposites which are obtained from these combinations were exemplified for improving their electrical, optical, and magnetic properties [36] as well as tribological, corrosion-resistance and other protective properties. As a significant point, when designing ceramic-metal nanocomposites, binary phase diagram of the mixtures should be considered and measures have to be taken to prevent a chemical reaction between ceramic and metallic components because the metallic component may easily react with the ceramic and thereby lose its metallic character [37]. Ceramic matrix composites are generally used for materials applications which require high temperature resistance, high strength, and erosion or wear resistance. The concept of ceramic-matrix nanocomposites was also applied to thin films which are solid layers of a few nm to some tens of μm thickness deposited upon an underlying substrate and that play a main role in the functionalization of technical surfaces.

2.1.3. Applications of the Nanocomposites

Nanocomposites are currently being used in a number of fields and new applications are being continuously developed. Because of the improved thermal and mechanical properties, nanocomposites are widely used in aerospace, automotive and thin film production applications. Besides, because of the improved electrical properties, nanocomposites are used in many electrical applications such as, thin-film capacitors for computer chips, solid polymer electrolytes for batteries, automotive engine parts, fuel tanks and conductive films. For the polymer-matrix cases, on the other hand, nanocomposites are generally used in food packaging, drug delivery and tissue engineering applications. Below are the some applications in which nanocomposites are being used, in detail.

2.1.3.1. Aerospace Applications

The usage of nanocomposite structures in commercial and general aviation aircraft has been increasing day by day because of the benefits that composites offer over

metal such as, better fatigue performance, lower weight, high corrosion resistance, tailorable mechanical properties, better design flexibility, lower assembly costs [38]. Besides, nanocomposites offer advanced solutions in aircraft construction. For example, they act as strengthening elements for the structures such as frames or stringers or as the outer layer for honeycomb type structures which are used at fuselage and wings. On the other hand, zirconia-based nanocomposites were used as thermal protection for turbo engines. They are also used as brake disk materials and brake lining for military and civil aircraft. Besides, nanocomposites serve a unique solution for the radoms of the hypersonic airplanes when combined with nanoadditive integrated ceramic matrix [39]. Recent developments in aircraft design, which can be seen in the Bombardier C-series, Airbus A380 and Boeing B787 airliners, have led to a blazing rise in the usage of nanocomposites and a corresponding increase in adhesive bonding of primary nanostructures in the aircraft [39-40].

2.1.3.2. Food Packaging

Nowadays, nanocomposites are currently developed to be used in food packaging applications because traditional packaging materials are not degradable and eco-friendly. On the other hand they have low mechanical and barrier properties. To overcome these problems, researchers have been investigating novel nanocomposites in food packaging area [41-42].To set an example, oxygen scavenger films were successfully developed by Xiao-e et al., by adding titania nanoparticles to different kind of polymers and the authors suggested their use for packaging a wide variety of oxygen-sensitive products [43]. For another example, Qi et al. have reported antibacterial activity of nanoscale chitosan when it is used with starch [44]. Besides, antibacterial effect with high mechanical strength of nanocomposites was investigated by many researchers [45-46]. All in all, the usage of nanocomposites in food packaging area is being developed day by day.

2.1.3.3. Electrical Applications

In recent years, nanocomposites have attracted an increasing interest in various fields and wide applications such as sensors, electrolytes, capacitors and conductive films owing to their unique electrical properties.

Production of conductive films is one of those fields and many researches had been performed about it. For example, Gao et al. had demonstrated a study about preparation of compact polypyrrole (PPy) polymer films embedded with different cobalt nanoparticles (CoNP) loadings by using electropolymerization process. At the end, it was seen that the multifunctional PPy/Co PNCs showed superparamagnetism, semi-conductive transportation and special dielectrical property at room temperature [47]. Another study was performed about preparation of nanocomposites in the form of flexible films with nanofibrillated cellulose (NFC), polyvinylpyrrolidone (PVP) and silver nanoparticles (AgNPs) by Khalil et al. After completing all characterization studies, it was demonstrated that the loaded nanocomposites with AgNPs showed promising electrical conductivity for various applications [48]. Besides, organic polymer based thermoelectric films consisting of poly(3,4-ethylenedioxythiophene):poly(styre nesulfonate) (PEDOT:PSS) with inorganic tin selenide (SnSe) nanosheets were fabricated in a study demonstrated by Ju et al. The results of this study showed that the introduction of inorganic SnSe nanosheets in the PEDOT:PSS conducting polymer and the subsequent treatments of the composite films are an efficient and promising strategy to obtain high-performance thermoelectric composites [49].

All of the studies which are mentioned above showed that nanocomposites are highly preferred in conductive film applications which require improved electrical properties.

2.1.3.4. Tissue Engineering Applications

Recently, scaffold-based tissue engineering approach has emerged as a promising strategy to create neo-organs and meet the growing clinical demand for the repair and regeneration of damaged tissues and/or organs. Scaffolds are the materials that have been engineered to cause desirable cellular interactions to contribute to the formation of new functional tissues for medical purposes and cells are often 'seeded' into these structures capable of supporting 3D tissue formation. Therefore, scaffolds should be biocompatible, biodegradable, non-toxic and they should provide good mechanical (especially good tensile) properties. In this manner, various nanocomposite biomaterial scaffolds mimicking the extracellular matrix (ECM). In the literature, various techniques have been used to produce nanocomposite tissue scaffolds such as, 3D printing (stereolithography, laser printing, fused deposition modeling, etc.),

solvent casting method, hybrid technologies, electrospinning, and combination of conventional methods with recent technologies [50-52]. Researchers had performed many studies about production of the scaffolds prepared by nanocomposites. As an example, 3D fully biodegradable and nanocomposite scaffolds for bone tissue regeneration, consisting of poly(ε-caprolactone) (PCL) reinforced with hydroxyapatite (HA) nanoparticles, were developed using an additive manufacturing process by Ronka et al. At the end, it was demonstrated that the introduction of HA strongly improved the compressive mechanical properties as well as the biological performance of the scaffolds in terms of cell adhesion and spreading [53]. Similary, Ozkan et al. performed a study about development of hybrid PCL/chitosan scaffolds with complex micro fibers/macro porosity by combining two different fabrication methods; electrospinning and solvent casting. At the end, it was suggested that the developed scaffolds were highly biocompatible and suitable candidates to be used in tissue engineering applications [54]. Likewise, Marino et al. had prepared gelatin/cerium oxide nanoparticles (nanoceria) nanocomposite fibers as antioxidant scaffolds for neuronal regeneration. Their study showed that obtained nanocomposite scaffolds represented a promising approach for nerve tissue engineering and regenerative medicine [55]. Additionally, El-Kady et al. aimed to fabricate novel silver releasing nanocomposite scaffolds, for bone treatment, by the gas foaming/particulate-leaching technique. Silver doped bioactive glass nanoparticles were used as a filler, to provide the scaffolds with bioactivity, as well as anti-bacterial properties in this study. At the end, it was suggested that developed scaffolds had anti-bacterial effects on agar plates; therefore they could be used for bone treatment [56].

Consequently, in tissue engineering (especially scaffold-based tissue engineering) applications, nanocomposites are the most suitable materials to produce a scaffold. Besides, among all other scaffold production techniques, electrospinning is the most widely used one. The most significant advantage of an electrospinning process is; high surface area to volume ratio can be easily obtained to speed up thermodynamic processes that minimize free energy. On the other hand, wide variety of polymers and materials can be used to form nanofibers. By electrospinning, fiber functionalization can be easily done. What's more, it is easy to combine different

materials to obtain complex/hybrid structures. Lastly, among all other techniques, electrospinning process requires relatively low start-up cost [10].

2.2. Electrospinning Process

Electrospinning is a technique which utilizes electrical forces for the production of polymeric fibers with diameters ranging from 2 nm to various micrometers by using polymer solutions of both natural and synthetic polymers, and melts. It is a commonly used technology for electrostatic fiber formation which has gained research and commercial attention over the past decade [10].

The effect which high voltage has on a polymer solution is the major principle of an electrospinning process. Basically, an electrospinning system consist of three main parts; a source of high voltage, a spinneret and a grounded collector. In this system, high voltage is connected to end of a capillary which contains liquid solution. Hemispherical surface of the liquid at the end of the capillary extends when the electric field intensity increases, and creates a Taylor cone which is a conical shape. The strand of polymer solution undergoes a process of instability and lengthening, while solvent evaporates and then the fibers are deposited on the collector [57]. An electrospinning process should be carried out under a ventilated chamber due to the possibilities of undesirable or harmful emissions of some polymers or solvent vapors occur during the process.

In this manner, electrospinning is one of the simplest ways to create nanofibers, but there are various parameters that can significantly affect the structure and formation of obtained nanofibers.

2.2.1. Parameters Affecting the Process

In an electrospinning process, there are several parameters that influence the structure/morphology/properties of obtained material. In the most basic case, these parameters are divided into three groups which are solution parameters such as concentration, molecular weight, conductivity, viscosity; process parameters such as applied voltage, capillary collector distance and flow rate and the ambient parameters such as humidity and temperature.

2.2.1.1. Solution Parameters

Concentration

The concentrations of polymer solution play a vital role in the fiber formation during an electrospinning process. If the concentration is very low, polymeric micro/nano particles may be obtained. In this case, instead of electrospinning, electrospray occurs because of the low viscosity and high surface tensions of the solution. If the concentration of the solution is a little higher, then a mixture of beads and fibers can be obtained which is not desired for an electrospun structure. Therefore, an optimum suitable concentration is required for an electrospinning process, thus smooth fibers could be obtained [58].

Molecular Weight

Another significant effect on morphologies of electrospun fibers is molecular weight of the polymers, because molecular weight reflects the entanglement of polymer chains in the solutions, which has an important effect on solution viscosity. Keeping the concentration fixed, while lowering the molecular weight of the polymer, can cause to form beads rather than smooth and desired fibers. Although smooth fibers can be obtained by increasing the molecular weight, further increasing can cause the formation of micro-ribbon [59].

Viscosity

For determining the fiber morphology, solution viscosity is the critical key. It has been proven that smooth and continuous fibers can not be produced, instead beads or beaded fibers are formed with very low viscosity, whereas very high viscosity may cause the hard ejection of jets from the solution, that's why an optimum and suitable viscosity is a requirement for an electrospinning process [60]. Principally, by adjusting the polymer concentration of the solution, the solution viscosity can be tuned; thus, several morphologies can be obtained. One thing should be noted that viscosity, polymer concentration, and polymeric molecular weight are related with each other.

Conductivity

Solution conductivity is another key factor that affects the fiber morphology and it is generally determined by the polymer type, solvent sort and the salt. Natural polymers are generally polyelectrolytic in nature, in which the ions increase the charge

carrying ability of the polymer jet, subjecting to higher tension under the electric field, resulting in the poor fiber formation in contrast to the synthetic polymers [61].

2.2.1.2. Process Parameters

Applied Voltage

Within the electrospinning process, applied voltage is the essential factor because charged jets can only be ejected from Taylor cone if the applied voltage higher than the threshold voltage. [10]. On the other hand, there are controversial arguments about the effects of applied voltage on fiber diameter and morphology. Several researchers suggested that higher voltages can cause the formation of large fiber diameter [18], whereas some others believe that the diameter of electrospun fibers was not affected by the applied voltage [62]. In addition to that phenomena, some research groups also demonstrated that higher voltage offers the higher possibility of bead formation while some researchers believe that bead formation can occur at low voltages due to the slower feed rate [63].

Capillary-Collector Distance

It has been proven that the distance between the capillary and the collector has an important effect on fiber diameter and morphologies. Concisely, if the distance is too short, the fiber will not have enough time to solidify before reaching the collector. On the other hand, if the distance is too long, beads can be formed in the structure. Moreover, it is well known that one important physical condition of the electrospun fiber is the dryness from the solvent, thus an optimum distance is recommended for an electrospinning process [64].

Flow rate

The flow rate of the working polymer solution within the syringe is another significant parameter since it is important to keep Taylor cone present and stable during the entire process. Generally, lower flow rate is more desirable and more recommended because the polymer solution can have enough time for polarization. On the contrary, if the flow rate is very high, bead fibers with thick diameter can be formed instead of smooth fibers with thin diameter due to the short drying time prior to reaching the collector and low stretching forces [65].

2.2.1.3. Ambient Parameters

Ambient parameters can also affect the fiber diameters and morphologies such as humidity and temperature. For example, Mituppatham et al. [66] had indicated that increasing temperature causes the thinner fiber diameter with polyamide-6 fibers for the inverse relationship between the solution viscosity and temperature. On the other hand, as for the humidity, low humidity may dry the solvent totally and increase the velocity of the solvent evaporation. On the contrary, high humidity can lead to the thick fiber diameter due to the charges on the jet can be neutralized and the stretching forces become smaller [67].

2.2.2. Types of Electrospinning Setups

In a simple and basic electrospinning process, the setup consists of three major components; a high voltage power supply that generates an electric field, a conductive spinneret and a collector. In general, the most basic experimental electrospinning setups can be classified as vertical (Figure 1) and horizontal (Figure 2), with respect to the layout with a single spinneret ejecting of liquid. Although these setups are the most widely used and the easiest ones, there are more specific and detailed setups which allow researchers to fabricate more complex nanofibrous structures in a more efficient way. If a suitable modification is applied to the electrospinning process or setup, nanofibers with some specific secondary structures can be prepared. Complex electrospinning was developed from basic electrospinning to fabricate nanofibers with secondary structures. In this manner, one of the developed setup is coaxial setup (Figure 3) and by using it, complex composite and/or hybrid fibers can be fabricated and these fibers are basically core-shell type single fibers obtained by coaxial spinning with two different spinning solutions which are drawn from a single capillary tip [68]. To put simple, by utilizing electrospinning with different setups, structural and morphological properties of the nanofibers can be changed to serve them in several applications.

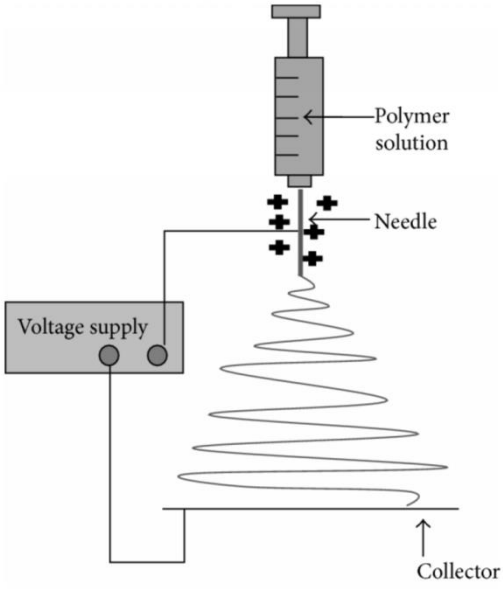

Figure 1. Vertical electrospinning setup.

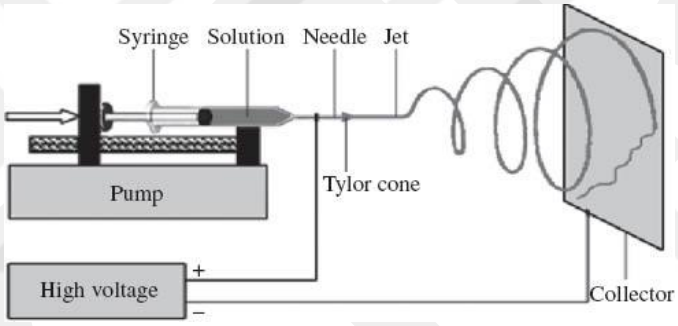

Figure 2. Horizontal electrospinning setup.

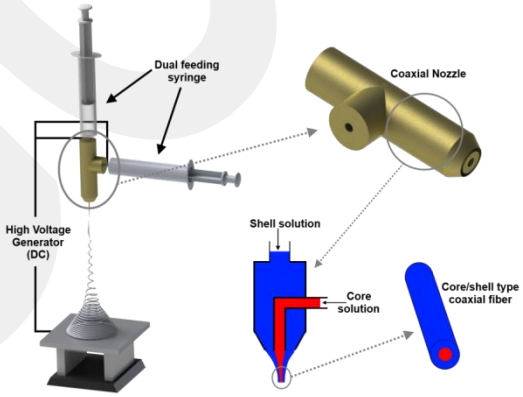

Figure 3. Coaxial electrospinning setup with a modified nozzle. One syringe to feed the core and the other to feed the shell solution.

2.2.3. Applications of Electrospinning

Due to the benefits of electrospinning process, which were mentioned above, it is a commonly used technique to fabricate nanofibers/nanocomposites by a wide range of polymers. These nanofibers/nanocomposites are widely used in several applications such as; filtrations, affinity membranes and recovery of metal ions, wound healing, release control, enzyme and catalyst carriers, ***electrical applications,*** sensors, energy storage, food and ***tissue engineering***. For example a study, performed by Chen et al., on using polyacrylamidoxime (PANOx)-containing PAN nanofibers for hydrolysis of p-nitrophenyl acetate (PNPA) indicated that diffusion resistances among the nanofibers might limit the accessibility of oxime catalytic sites in the fiber and by this way, influence the catalytic activity [69]. In another study, a gas sensor using a specific absorption interaction between ammonia and poly(acrylic acid) (PAA) nanofibers was indicated, and weight difference induced by the gas absorption was measured by a quartz crystal microbalance (QCM). At the end of the study, the sensor obtained by electrospinning process was capable of detecting ppb level NH_3 in the air, and the sensitivity was four times higher than that of the PAA cast film [70]. On the other hand, nanofibers obtained by electrospinning are mostly used in tissue engineering applications since the morphology of the obtained fibers is very similar to the extracellular matrix (ECM) of the natural tissue. Electrospun fibers are porous and thanks to electrospinning, it is possible to adjust the pore size, morphology or the amount. Hence, it is possible to create a scaffold that supports cell attachment, 3D proliferation and growth. As an example, Wang et al., demonstrated a study in which silk fibroin/gelatin composite vascular scaffold, prepared by electrospinning to be used in blood vessel tissue engineering, demonstrated long term cell adhesion, proliferation and growth with no toxicity during in vitro cell culture [71]. As a conclusion, among all literature survey showed that the electrospinning process is widely used as a beneficial and effective technique to create nanofibers for several applications.

2.3. Poly(vinyl alcohol)

PVA is a colorless, synthetic and water-soluble polymer containing large amounts of hydroxyl groups. It has the idealized formula $[CH_2CH(OH)]_n$. Unlike most vinyl polymers, PVA is not prepared by polymerization of the corresponding monomer. The monomer, vinyl alcohol, is unstable with respect to acetaldehyde. Instead, PVA

is prepared by first polymerizing vinyl acetate, and the resulting polyvinyl acetate is converted to the PVA, which makes PVA unique among other polymers [14].

PVA has a melting point of 230 °C and 180–190 °C for the fully hydrolyzed and partially hydrolyzed grades, respectively. It has a glass transition temperature (Tg) of 85°C and it rapidly decomposes above 200 °C because it can undergo pyrolysis at high temperatures. At room temperature, PVA has an amorphous density of 1.26 g/cm^3 and crystalline density of 1.35 g/cm^3, respectively [15].

The strong and the small size hydrogen bond interactions of the hydroxyl groups in PVA molecule force the polymer chains into a crystal lattice, thus PVA is being partially crystalline. On the other hand, PVA has excellent oxygen barrier properties. It has grease, oil and organic solvent resistance and low moisture permeability and it is stable against UV radiation [72]. Besides, PVA is a non-toxic, biodegradable and biocompatible polymer as well as it has high durability.

Consequently, all beneficial properties of PVA mentioned here let it be used in various applications such as films, membranes, binders in the paper industry, adhesives, textile, drug delivery, food engineering and tissue engineering [72-73].

Fibers and the thin films obtained from PVA have the same excellent biologically properties and moreover, they have high tensile properties and high abrasion resistance. Therefore, PVA is a commonly used polymer in tissue engineering applications, especially in scaffold preparation. For instance, macroporous PVA scaffold was utilized to promote deposition and growth of mineral layers using the biomimetic approach by Ye et al and the results from this study suggested that mineralized PVA scaffold could be utilized to develop in vitro model of breast cancer bone metastasis [74]. Further, in another study, novel electrospun gellan based nanofibers as a hydrophilic scaffolding material were fabricated using a blend mixture of gellan with PVA [75]. At the end, it was seen that these fabricated nanofibers proved to exhibit good uniformity, structural integrity and cytocompatibility.

Over and above, PVA is used for many other applications because of its excellent thermal properties. For example, Esmaili et al. designed a novel fixed-bed reactor with a nanofiber membrane composed of a PVA/chitosan nanofiber blend prepared

by electrospinning technique [76]. The results from this study showed that the obtained PVA/chitosan nanofibers were suitable candidates for a successful metal ion removal in a novel fixed-bed reactor. Likewise, Liu et al. presented a novel class of high-flux microfiltration filters consisting of an electrospun nanofibrous membrane and a conventional non-woven microfibrous support fabricated by electrospinning of PVA [77]. At the end, it was concluded that the prepared electrospun PVA membrane can potentially be an excellent and effective candidate to remove bacteria, microorganisms or microparticles from waste water with a relatively low cost.

Among all these literature survey, it was understood that PVA is a commonly used polymer for various applications due to its biological, mechanical and thermal properties.

2.4. Graphene

Graphene can be defined as the allotrope of carbon and 2D sheet of sp^2 bonded carbon atoms which are arranged in a honeycomb hexagonal lattice (Fig. 4). Graphene is the fundamental structural element of other allotropes, including graphite, carbon nanotubes and fullerenes. Graphite takes form due to layers of graphene stacked around each other in a 3D framework and when this framework is separated into a flat 2D network of layers, graphene is developed. Besides, it is the only 2D framework composed of only carbon. Graphene is also considered as an indefinitely large aromatic molecule, the latest case of the family of flat polycyclic aromatic hydrocarbons [78].

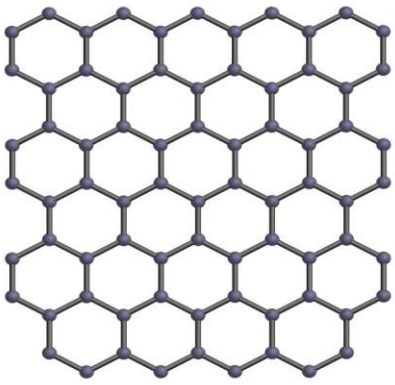

Figure 4. Schematic representation of a graphene lattice.

Because of its unique properties, graphene has been known as an allotrope which has attracted much attention from scientists both in the industry and academia, in the past decade [78-79]. It is almost 100 times stronger than the strongest steel in the world and it is almost transparent. Graphene is not only being the lightest, thinnest, and strongest known material, but also it provides flexibility and extremely high thermal and electrical conductivity. With these unique properties and features, graphene has been used in several applications such as, flexible and wearable electronics and antennas, flexible displays, pressure sensor design, optoelectronics, medical, bioengineering and nanoengineering technologies, rechargeable batteries and photovoltaics [80-81].

To utilize graphene's properties in the most effective way for a wide-ranging amount of potential applications, graphene can be produced and used in different forms.

2.4.1. Graphene Oxide (GO)

Graphene oxide can be defined as a chemically modified graphene which is prepared by oxidation and exfoliation, and is a monolayer material with high oxygen content, thus monolayer flakes can be found in the structure of GO [82].

One of the main advantages of GO is, it can be easily dispersed in water and different matrixes, as well as in other organic solvents, due to the presence of the oxygen functionalities. This remains as a one of the most significant property when mixing the material with ceramic or polymer matrixes while trying to improve their electrical and mechanical properties [83].

GO’s properties can be fundamentally changed by functionalization. The obtained chemically modified and/or functionalized graphene could potentially become much more adaptable for various applications. Depending on the desired applications or properties, there are many ways in which graphene oxide can be functionalized. For instance, it is possible to substitute amines for the organic covalent functionalization of graphene to increase the dispersibility of chemically modified graphene in organic solvents for optoelectronics, bio-devices or as a drug-delivery material [80-83]

On the other hand, it is important to develop an oxidization and reduction process that is able to separate individual carbon layers and then isolate them without

modifying their structure in order for graphene oxide to be usable in many applications.

2.4.1.1. Reduced Graphene Oxide (rGO)

Reducing graphene oxide to obtain rGO is an extremely important process because it has a large impact on the quality of the rGO produced, and therefore will determine how close rGO will come, in terms of structure, to pristine graphene. When it is considered in large scale operations where scientists and engineers need to apply large quantities of graphene for scientific and industrial applications such as energy storage, rGO is the most effective solution, because of the relative ease in creating sufficient quantities of graphene to required quality levels to be used in desired applications [84]. There are a number of reduction procedures of GO, though they are all methods based on chemical, thermal, microwave, photo-chemical, photo-thermal or microbial/bacterial means [84-85].

Latterly, in terms of nanocomposites, rGO is attracted by many researchers because of its high quality and its beneficial usage in many applications such as electronics, food engineering and biotechnology. For example, a study about preparation of silver nanoparticle-reduced graphene oxide decorated electrospun polyurethane fiber composites was demonstrated by Liu et al. The results of this study demonstrated an effective strategy to harvest metal nanoparticle-graphene hybrid material reinforced polymer composites that are lightweight, highly flexible and have an excellent electrical property to be used in flexible electronic products [78]. Moreover, another study was performed by Pal et al. and it was aimed to develop a nanocomposite film with cellulose nanocrystals (CNC)/rGO as reinforcing nanofillers incorporated into polylactic acid (PLA, polymer matrix) by solution casting method and to examine its potential in packaging, barrier and medical applications. At the end, the results of this work demonstrated that the good dispersion of CNC and rGO is feasible within the PLA matrix with high tensile strength and thermal stability in addition to antibacterial response and high biocompatibility [18].

Conclusively, once rGO has been produced, there are many ways that rGO can be functionalized to be used in several applications. By treating rGO with other chemicals or by creating new compounds/composites/materials by combining rGO

with other materials, the properties of the obtained material can be enhanced to suit commercial applications.

2.4.2. CVD-Grown Graphene

There are several ways in which graphene monolayer can be isolated or created, but the most popular process is chemical vapor deposition so far. By CVD process, relatively high quality graphene can be produced, especially on a large scale. The CVD process is moderately straightforward, but in some cases, some specialist equipment is necessary. For a CVD process, it is important to follow guidelines set carefully, concerning pressure, temperature, gas volumes, and time duration in order to create good quality graphene [86-87].

In general and the simplest manner, CVD can be defined as a way of depositing gaseous reactants onto a substrate. The working principle of CVD combines gas molecules, which are often used as carrier gases, in a reaction chamber that is typically set at ambient temperature. When the combined gases contact with the substrate in the heated reaction chamber, a reaction occurs to create a material film on the surface of the substrate. Then, the waste gases are pumped from the reaction chamber. In that point, it is significant to set the temperature correct, since the temperature is an elementary factor which defines the type of reaction that occurs [88-89].

Creation of CVD graphene is generally done in two steps, the precursor pyrolysis of a material to form carbon, and the carbon structure formation of graphene by using disassociated carbon atoms. The first step must be carried out on the surface of the substrate to prevent the precipitation of carbon clusters during the gas phase. Pyrolytic decomposition of precursors needs to be performed on extreme levels of heat; therefore by using metal catalysts, the reaction temperature must be reduced. The second phase of creating out the carbon structure of the disassociated carbon atoms also requires a very high level of heat, so using a catalyst is mandatory to reduce the temperature needed for a reaction, at this stage. The problem with using catalysts is introducing more compounds into the reaction chamber that will have effects on the reactions. One example of these effects is the way the carbon atoms dissolve into certain substrates such as Nickel during the cooling phase.

Simply put, it is vital that the CVD process is very rigorously coordinated, and the controls are put in place at every stage of the process to ensure that the reactions occur effectively, and that the quality of graphene produced is of the highest attainable. Because of the obtained high quality graphene, CVD grown graphene is commonly used in many applications such as; filtration, electrical applications, sensors, electrodes and catalytic applications, nanoengineering and bioengineering technology [90-92].

CHAPTER 3
Experimental Study

3.1. Materials

PVA (average molecular weight, 85,000 g.mol^{-1}-124,000 g.mol^{-1} and HD, 87%-89%) was purchased from Sigma-Aldrich and used without further purification. rGO is commercially purchased from Graphenea, Spain. CVD-grown monolayer graphene was obtained from Sabanci University Nanotechnology Research and Application Center (SUNUM), Sabanci University, Turkey. Phosphate buffer saline (PBS) was obtained from Amresco (USA). For cell culture studies, PBS (phosphate buffer saline) and BSA (bovine serum albumin) were obtained from Amresco (USA), Dulbecco's Modified Eagle Medium (DMEM/F12), penicillin/streptomycin, fetal bovine serum (FBS), ethanol (96%, v/v), Alizarin Red-S and Alkaline Phosphates Kits were purchased from Sigma-Aldrich (USA). Besides, the stain 4′,6-Diamidino-2-phenylindole dihydrochloride (DAPI) was purchased from Sigma-Aldrich (USA).

3.2. Preparation of the Nanocomposites

3.2.1. PVA+rGO Nanocomposites

3.2.1.1. Preparation of the Solutions

In order to prepare electrospun PVA, PVA+0.5 wt% rGO and PVA+1.0 wt% rGO nanocomposites, solution parameters were determined with the help of literature. After detailed literature survey, following solution parameters were applied. Briefly, 2 g PVA powder was dissolved in 30 ml distilled water and magnetically stirred at 90°C for 3 hours [93]. Afterwards, rGO was added to the PVA mixtures and magnetically stirred for 5 hours. At the end, the concentration of rGO in the solution was 0.5 and 1.0 wt%. After all, it was seen that rGO was homogenously dispersed in the PVA solutions.

3.2.1.2. Optimization and Determination of Electrospinning Process

In order to produce electrospun PVA, PVA+0.5 wt% rGO and PVA+1.0 wt% rGO nanocomposites, electrospinning process parameters, which are feeding rate, voltage and the needle-collector distance should be determined. In order to prepare electrospun PVA mats, PVA+0.5 wt% rGO and PVA+1.0 wt% rGO nanocomposites, electrospinning process parameters were optimized. For that, the obtained polymer solutions were fed into a 5 ml syringe and the syringe was attached to the pump. To optimize the electrospinning parameters for electrospun PVA, PVA+0.5 wt% rGO and PVA+1.0 wt% rGO nanocomposites, a serial number of experiments had been done. The optimization studies for PVA+0.5 wt% rGO and PVA+1.0 wt% rGO nanocomposites were shown in Table 1 and 2, respectively.

Table 1. Electrospinning process parameters of PVA+0.5 wt% rGO.

Experiment No	Needle-Collector Distance (cm)	Feeding Rate (µL/min)	Voltage (kV)	Observation
1	6	10	15	Not-spinned
2	6	10	20	Not-spinned
3	6	10	25	Not-spinned
4	6	15	15	Not-spinned
5	6	15	20	Not-spinned
6	6	15	25	Not-spinned
7	6	17	15	Needle-spinned
8	6	17	20	Needle-spinned
9	*6*	*17*	*22*	*Spinned*
10	6	17	25	High voltage

Table 2. Electrospinning process parameters of PVA+1.0 wt% rGO.

Experiment No	Needle-Collector Distance (cm)	Feeding Rate (µL/min)	Voltage (kV)	Observation
1	6	10	15	Not-spinned
2	6	10	22	Not-spinned
3	6	10	25	Not-spinned
4	6	15	15	Not-spinned
5	6	15	20	Not-spinned
6	6	15	25	Not-spinned
7	6	17	15	Not-spinned
8	6	17	20	Not-spinned
9	6	17	22	Not-spinned
10	6	17	25	High voltage
11	8	10	15	Not-spinned
12	8	10	20	Not-spinned
13	8	10	22	Not-spinned
14	8	15	15	Not-spinned
15	8	15	20	Not-spinned
16	8	15	22	Not-spinned
17	8	15	25	Not-spinned
18	10	10	15	Not-spinned
19	10	15	15	Not-spinned
20	10	17	15	Needle-spinned
21	10	20	15	Not-spinned
22	10	10	20	Not-spinned
23	10	15	20	Not-spinned
24	10	17	20	Needle-spinned
25	10	10	22	Not-spinned
26	*10*	*15*	*22*	*Spinned*
27	10	17	25	High voltage

3.2.2. PVA Electrospun CVD-Grown Monolayer Graphene Nanocomposites

3.2.2.1. Synthesis of Monolayer Graphene

CVD-grown monolayer graphene used in this study was donated from SUNUM, Turkey. The following procedure was applied to obtain it. Briefly, monolayer graphene was synthesized by CVD method using 25 µm thick copper (Cu) foil as a catalyst as described in the literature [91]. The copper pieces were put into a quartz chamber and heated to the 1035°C under vacuum in 80 standard cubic centimeter per minute (sccm) H_2 and annealed for 30 min. After annealing a 40 sccm CH_4 flow was

added to the H_2 flow. Then, 30 min graphene growth was carried out cooling down with H_2 flow until the temperature was below 100 °C.

3.2.2.2. Preparation of PVA Solution

In order to prepare PVA electrospun CVD-grown monolayer graphene, the solution of PVA was prepared as described in Section 3.2.1.1.

3.2.2.3. Determination of Electrospinning Process

In order to produce PVA electrospun CVD-grown monolayer graphene, electrospinning process parameters, which are feeding rate, voltage and the needle-collector distance, should be determined. To obtain electrospun PVA mats, the process parameters were determined from the literature [93]. Afterwards, PVA solution was electrospun onto monolayer graphene and electrospinning parameters of PVA onto CVD-grown monolayer graphene were determined in Section 3.2.1.2. with the help of literature.

3.3. Production of the Nanocomposites

To obtain electrospun PVA, PVA+0.5 wt % rGO, PVA+1.0 wt % rGO and PVA electrospun CVD-grown monolayer graphene nanocomposites, electrospinning method was applied with the previously determined/optimized solution and process parameters. For the production of PVA mats and PVA+rGO nanocomposites, 2 g of PVA powder was dissolved in 30 ml distilled water and magnetically stirred at 90°C for 3 hours, and then rGO was added to the PVA mixtures and magnetically stirred for 5 hours with the concentration of rGO in the solution as 0.5 and 1.0 wt% as the higher rGO content in the matrix can cause toxicity for several applications such as tissue engineering and food packaging. To prepare PVA mats, with the help of literature, electrospinning parameters were found as; the distance between needle and the collector was 20 cm, voltage was 20 kV and the feeding rate 6.7 μL/min. For the preparation of PVA+0.5 wt % rGO nanocomposites, electrospinning parameters were determined as; the distance between needle and the collector was 6 cm, voltage was 22 kV and the feeding rate was 17 μL/min. For PVA+1.0 wt % rGO nanocomposites, electrospinning parameters were determined as; the distance between needle and the collector was 10 cm, voltage was 22 kV and the feeding rate was 15 μL/min. On the other hand, to prepare PVA electrospun CVD-grown monolayer graphene nanocomposites, firstly monolayer graphene was synthesized, and then a PVA

solution was prepared. Later, Cu foil with CVD-grown graphene was fixed on the collector in the electrospinning set-up and the PVA solution was electrospun onto CVD-grown monolayer graphene with the solution and electrospinning parameters mentioned above. Lastly, the electrospun PVA structure was peeled-off from Cu foil like a scotch tape to transfer the graphene onto electrospun PVA structure. All of the experiments were carried out at room temperature.

3.3.1. Crosslinking of the Nanocomposites

PVA is the most widely produced water-soluble synthetic polymer in the world [94]. Super-hydrophilic character and water-soluble property of PVA restrict its usage in many applications. To overcome this problem, electrospun nanofibers were cross-linked to have a stable and robust material. The obtained nanofibers were cross-linked by using UV-light of 253.7 nm (UV-340 lamp) at 30 W with different durations (15, 30, 45, 60 and 75 min) and then they were kept in both water and PBS solutions to optimize the crosslinking duration.

3.4. Characterizations

3.4.1. Thickness Measurements

The thicknesses of electrospun PVA mats, PVA+0.5 wt % rGO, PVA+1.0 wt % rGO and PVA electrospun CVD-grown monolayer graphene nanocomposites were measured using a micrometer (outside micrometer, 0-25 mm, USA) and the average values were calculated from 6 measurements of different samples for the same sample batch.

3.4.2. Contact Angle (CA) Measurements

The contact angle values of electrospun PVA mats, PVA+0.5 wt % rGO, PVA+1.0 wt % rGO and PVA electrospun CVD-grown monolayer graphene nanocomposites were measured as a function of surface tension of a series of liquids by using the sessile drop water contact angle measurement system (Phoenix 300, Surface Electro Optics, South Korea). Three samples were employed for each test, the average and the standard deviation values were calculated for each sample and compared to the reference surface wettability of commercial TCPS (Tissue Culture Polystyrene).

3.4.3. Optical Microscopy Analyses

The optical microscopy images of CVD-grown monolayer graphene at Cu foil before and after peeling-off process (Cu foil only) were taken by an optical microscopy (Omano Light Microscopy, USA), to control transfer of the CVD-grown monolayer graphene from the Cu foil.

3.4.4. Scanning Electron Microscopy (SEM) Analyses

Scanning Electron Microscope (Quanta 400F SEM, FEI, USA) was used to examine obtained nanocomposites (observations of morphologies and transfer of CVD-grown monolayer graphene). Before analyses, the samples were coated with gold. The average fiber diameter and the average inter-fiber pore size values were calculated via ImageJ Launcher software program (USA) using SEM photographs. For the evaluation, 8 images of each sample were used and at least 30 measurements were taken and the results were statistically evaluated by JStats 1.8 software.

3.4.5. Mechanical Properties

The electrospun nanocomposites were cut into dog-bone shapes (40 mm x 5 mm) and the mechanical properties were obtained with a universal tensile testing instrument (Zwick/Roell 250 kN, Germany) with 100 N load cell with a speed of 10 mm/min at room temperature. Electrospun PVA mats were used as control group for mechanical evaluation.

3.4.6. Attenuated Total Reflection Fourier Transform Infrared Spectroscopy (ATR-FTIR) Analyses

The chemical compositions of commercial rGO, electrospun PVA mats, PVA+0.5 wt % rGO and PVA+1.0 wt % rGO nanocomposites were determined with ATR-FTIR spectrometer (Bruker Vertex 70, Germany) with a scan resolution of 2 cm^{-1} in the range from 4000 to 500 cm^{-1} in order to obtain characteristic peaks of the materials and to observe interactions between PVA and rGO.

3.4.7. Thermogravimetric (TGA) Analyses

The TGA analyses were performed in a TGA thermo-analyzer (Perkin Elmer Pyris 1 TGA, USA) instrument. The loss of weight was monitored from 25°C to 700°C with

a heating rate of 10°C min^{-1} under a nitrogen gas flow. Electrospun PVA mats were used as control group for TGA evaluation.

3.4.8. X-Ray Diffraction (XRD) Analyses

XRD studies (Ultima IV, USA) of the commercial rGO, electrospun PVA mats, PVA+0.5 wt % rGO and PVA+1.0 wt % rGO nanocomposites were conducted with a Cu-Kα radiation in the scanning range of 1-50° of 2Θ with a scanning speed of 0.5° min^{-1}.

3.4.9. Raman Analyses

The Raman spectra of electrospun PVA, neat CVD-grown monolayer graphene (CVD-grown monolayer graphene at Cu substrate) and PVA electrospun CVD-grown monolayer graphene were recorded with a Raman spectrometer (Renishaw inVia) with an incident laser beam wavelength of 532 nm.

3.4.10. PBS Absorption and Shrinkage Tests

For shrinkage and PBS absorption characteristics determination, at first nanocomposite samples were cut into rectangular shaped pieces with the dimensions of 10 mm x 5 mm. Then, the samples were put in the bottles containing 20 ml of PBS (pH = 7.4) and they were in vitro incubated for 24 h at 37.0 ˚C. After the incubation period, the samples were removed from PBS and they were blotted with a filter paper to remove the excess water on the surface. Then after, the weights of the samples were measured. With the formula below, the water uptakes of the samples in PBS were calculated.

$$A(\%) = \left(\frac{W_1 - W_0}{W_0} \right) x100$$

Here, A is the PBS absorption (%), W_0 (g) and W_1 (g) are the weights of the nanocomposites before and after immersion in PBS medium for 24 h, respectively. For each group, three samples were recovered after they were being incubated in PBS and then dried in a vacuum oven for 12 h to remove the excessive water on them. The sizes of the dried samples were measured, the surface areas were calculated and finally, they were compared with the initial areas. Consequently, the shrinkage percentage was measured as the change ratio of the surface area change of the recovered samples.

3.4.11. In Vitro Degradation

The in vitro degradation analyses of the nanocomposites were performed by using ASTM F 1635-04 method [95]. The nanocomposite samples were weighed and immersed in 0.1 M PBS with pH 7.3, with three replicas containing 58.100 units/ml of lysozyme. The storage of the samples was performed in test tubes, kept in an incubator at 37 ˚C. After 1, 30, 60, 90, 120, 150 and 180 days period of incubation, the samples were removed from the medium and washed with distilled water and dried in vacuum oven for 24 h to remove excess water and weighed. The weight remaining was calculated with the below formula.

$$Weight\ remaining\,(\%) = 100 - \left(\frac{W_0 - W_d}{W_0} \times 100 \right)$$

W_0 and W_d are the weights of the electrospun scaffolds before and after degradation for a specific time interval, respectively.

3.4.12. Water Vapor Transmission Rate (WVTR)

Water vapor transmission rate of the prepared rGO/PVA nanocomposites was measured by using ASTM E96/E96M test method [96]. The results were obtained through the measurement of the weight loss of water in a bottle containing 10 ml of distilled water with a diameter of 50 mm. The samples with 2 mm of thicknesses and 50x50 mm of dimensions were tightly sealed on the mouth of the cylindrical cup. Then, the sealed cups were incubated at 37˚C for 24h. The WVTR was calculated by the following equation.

$$WVTR = \frac{W_0 - W_f}{A \times 24} x10^6 \ \text{g/m}^2\text{.day}$$

Where A is the mouth area of the bottle, W_0 (gram) and W_f (gram) are the weights of the bottle before and after the incubation, respectively.

3.4.13. Electrical Conductivity Measurements

Electrical conductivities of the electrospun PVA mats, PVA+0.5 wt % rGO, PVA+1.0 wt % rGO and PVA electrospun CVD-grown monolayer graphene nanocomposites were measured with a 4-point probe electrical conductivity device

(Keithley 220, USA). Electrospun PVA mats were used as control group for conductivity evaluation.

3.5. Cell Culture Studies

To observe cell-material interaction of the electrospun PVA mats, PVA+0.5 wt % rGO, PVA+1.0 wt % rGO and PVA electrospun CVD-grown monolayer graphene nanocomposites, the cell culture studies were performed by using MG-63 human osteosarcoma cell line (ECACC 86051601). $5x10^5$ cells/ml cell concentrations were seeded on the prepared nanocomposites and they were incubated under 5% CO_2 at 37°C and kept for 25 days. As a culture medium, DMEM/F12 + %10 (v/v) FBS + 1% (v/v) penicillin+streptomycin (100 units/ml penicillin, 100 μg/ml streptomycin) was used. The nanocomposites were cut as 1 cm diameter circular shape and they were sterilized with UV for 30 min. Then, the samples were placed in TCPS well. Cell viability was determined by MTT Assay, calcium deposition was detected by Alizarin Red Staining, the differentiation was determined by Alkaline Phosphates Activity (ALP); the adhesion growth and proliferation characteristics of the seeded nanocomposites were examined by fluorescence and SEM microscopy analyses. TCPS and electrospun PVA mats were used as control group for overall cell culture evaluation.

3.5.1. MTT Assay

To observe cell viability on the prepared nanocomposites, MTT (3-(4,5-dimethyl-2-thiazol)-2,5-diphenyl-2H-tetrazolium bromide) assay was performed. The samples were placed in parafilm coated 24 well-plates and MTT assay was carried out for 21 days of the culture out of 48 hours. The cell solution was added to each well and incubated for 24 hours. After the incubation, the seeded nanocomposites were removed from the incubator, the medium was discarded and the samples were washed with PBS for 3 times. After washing the samples, 600 μl fresh medium and 60 μl MTT solution were added to each well and incubated for an additional 3 hours. After the incubation, the MTT solution was aspirated, and formazan crystals that formed were dissolved in 1 ml dimethylsulfoxide (DMSO) and incubated for 1 hour. For the measurement, 200 μl solutions were taken from each well and placed into 96 well-plates. Eventually, the absorbance values were measured with a microplate reader at 540 nm and the cell viability was observed.

3.5.2. ALP Activity

The ALP activity of the cultured nanocomposites was measured on 7^{th}, 14^{th} and 21^{st} days of the cultivation. Briefly, BCIP/NBT tablet was dissolved in 10 ml distilled water to prepare the substrate solution. The solution was stored in the dark for 2 hours. The cultured samples were removed from the incubator, the medium was carefully aspirated and the cells were washed with PBS for 2 times. Afterwards, 10% formalin was added to cover the sample surface and kept for 60 sec. Then by, the formalin was discarded and the samples were washed with PBS. Substrate solution was added to the wells, incubated at RT for 5-10 min and the progress was checked every 2-3 min. After all, the values were measured with a spectrometer at 405 nm.

3.5.3. Alizarin Red Staining

In order to observe calcium deposition of the prepared and cultured nanocomposites, Alizarin Red Staining was performed. For that, 2 g of Alizarin Red stain was dissolved in 100 ml distilled water and pH of the solution was adjusted to 4.1-4.3 with HCL. Then, the obtained dark brown solution was filtered and stored in the dark. The samples were removed from the incubator, the medium was carefully aspirated and the cells were washed with PBS without disrupting the cell monolayer. This process was followed by the fixation of the cells with 10% formalin. After at least 30 min, the formalin was carefully aspirated and the cells were washed with distilled water. After discarding the distilled water, stain solution was added on the samples and they were incubated in the dark for 30 min. Then the stain solution was centrifuged at 200 rpm and the mineralization level was measured at 405 nm. Eventually, calcium depositions were seen in dark orange-red colors.

3.5.4. Fluorescence Microscopy Analyses

Fluorescence microscopy analyses ware performed to observe cell attachment and growth on/within the developed nanocomposites. The images were taken on 7^{th}, 14^{th} and 21^{st} days of the cultivation. For imaging, the cultured samples were taken from the incubator, the medium on the samples was carefully aspirated and the samples were washed with PBS for 3 times. Later, the samples were immersed in 0.1% Triton X-10 solution for 5 min to increase cell permeability. After discarding the Triton X-10 solution and washing the samples with PBS, the cells on/within the nanocomposites were stained with 10 mg/mL DAPI solution and kept in the dark for

15 min; and the images were taken with Fluorescent Microscope (AMG EVOS-FL, USA) immediately.

3.5.5. Observation with SEM

The morphological characteristics of the cells on the cultured samples were observed by SEM. For that, the medium in each well was discarded and the samples were washed 3 times with PBS. Following the fixation with 2.5% v/v paraformaldehyde for 30 min, the samples were dehydrated for 2 min sequentially with water/ethanol solutions with increasing ethanol content up to 100%. Finally, the samples were immersed in 100% hexamethyldisilazane for 5 min, air-dried and coated with Au-Pt (~3 nm) before the analyses.

CHAPTER 4

Results and Discussions

4.1. Production of the Nanocomposites

In order to obtain PVA, PVA+0.5 wt % rGO, PVA+1.0 wt % rGO and PVA electrospun CVD-grown monolayer graphene nanocomposites, solution and process parameters were either determined from the literature or optimized. The determined/optimized parameters mentioned in Section 3.2.1. and 3.2.2. were used to produce nanocomposites serially, which were used in further characterization studies.

4.1.1. Crosslinking of the Nanocomposites

After completing production step, the obtained fibrous structures were crosslinked by using UV-light of 253.7 nm (UV-340 lamp) at 30 W with different durations (15, 30, 45, 60 and 75 min) to make them stable and water resistant. Thereupon, complete crosslinking was seen for 75 min for electrospun PVA mats and PVA electrospun CVD-grown monolayer graphene, 60 min for PVA +0.5 wt % rGO nanocomposites and 45 min for PVA+1.0 wt % rGO nanocomposites as they were remained intact both in the water and PBS solutions for more than 1 month. From naked-eye observations and SEM images, it was seen that the crosslinking of UV-radiation did not destroy the morphology of the nanocomposites.

4.2. Characterizations

4.2.1. Thickness, the Average Fiber Diameter, the Average Inter-Fiber Pore Size and Porosity (%) Values

The thicknesses of electrospun PVA mats, PVA+0.5 wt % rGO, PVA+1.0 wt % rGO and PVA electrospun CVD-grown monolayer graphene nanocomposites were measured in the range of 0.053-0.054 mm. On the other hand, the electrospinnability is affected by polymer concentration, feeding rate, tip-to-collector distance, and applied voltage [74], thus the fiber diameters and the pore sizes are changed with the electrospinning process parameters. The average fiber diameters were measured by

using Image J Launcher software program (USA) with the help of SEM images. From the measurements (Table 3), it was seen that the highest fiber diameter belonged to electrospun PVA+0.5 wt% rGO (~388 nm) nanocomposites whereas the lowest fiber diameter was measured for the electrospun PVA mats (~340 nm). This is because a small amount of rGO into PVA solution moderated the viscosity, thus the fiber diameter increased for PVA+0.5 wt% rGO nanocomposites. However, increasing rGO content more, increased the electrical conductivity of the precursor, resulted smaller fiber diameter for PVA+1.0 wt % rGO nanocomposites [97]. Besides, the highest average inter-fiber pore size were measured as 1.076, 1.209 and 1.170 μm for electrospun PVA mats, PVA+0.5 wt % rGO, and PVA+1.0 wt % rGO nanocomposites, respectively. The results obtained here showed that there was an increase of pore sizes with the increase of fiber diameter and this phenomenon was also attributed by other researchers before [52,98]. Lastly, the highest porosity (%) was seen for electrospun PVA+0.5 wt % rGO nanocomposites (nearly the same, but a little more than PVA+1.0 wt % rGO nanocomposites) where the lowest porosity (%) was seen for electrospun PVA mats as it was expected from the literature [99]. In addition, for the case of PVA electrospun CVD-grown monolayer graphene nanocomposites, the results were identical with those of the electrospun PVA mats, as the main matrix was electrospun PVA for both.

Table 3. Properties of the nanocomposites *(p<0.0005)*.

Sample	Thickness (mm)	Average fiber diameter (nm)	Average inter-fiber pore size (μm)	Porosity (%)
Electrospun PVA	0.054±0.003	335±6.000	1.068 ± 0.120	79.400
Electrospun PVA+0.5 wt% rGO	0.053±0.012	388±5.004	1.209 ± 0.104	81.600
Electrospun PVA+1.0 wt% rGO	0.054±0.009	365±4.001	1.170 ± 0.050	80.400
PVA electrospun CVD-grown monolayer graphene	0.052±0.001	332±1.000	1.052 ± 0.020	79.100

4.2.2. Contact Angle (CA) (°) Measurements

The CA (°) values of the prepared materials were measured to determine their wettability characteristics and the results were provided in Table 4. As-spun PVA (without crosslinking), has a super-hydrophilic character itself, thus the CA value could not be measured [100]. On the contrary, UV-crosslinked electrospun PVA had a moderate wettability value and the CA of the electrospun PVA was measured as ~62°. This is, most probably, because of the orientation change of hydroxyl groups inside PVA chains by UV-radiation [101]. With the presence of rGO, on the other hand, lower CA values were obtained for the electrospun nanocomposites leading more hydrophilic structures due to the hydrophilic character of reduced graphene oxide owing functional O groups [98]. Consequently, the CA values for the electrospun PVA+0.5 wt% rGO and PVA+1.0 wt% rGO nanocomposites were measured as around ~53° and ~55°, respectively, which are close to the CA value of tissue culture polystyrene (TCPS) (~50°) [52]. In the literature it was reported that a wettability value which is close to the TCPS, supports cell adhesion and growth better [52], therefore rGO added nanocomposites were considered as suitable

candidates to be used in scaffold-based tissue engineering. On the other hand, the CA value of PVA electrospun CVD-grown monolayer graphene nanocomposites was measured as ~60° because of the moderate wettability characteristics of CVD-grown graphene [102]. Consequently, all of the prepared samples were appropriate candidate materials to be used in scaffold-based tissue engineering, as they all had the moderate wettability values.

Table 4. CA (°) values of the samples.

Sample	CA (°)
Electrospun PVA	62.100±1.250
Electrospun PVA+0.5 wt% rGO	53.210±1.102
Electrospun PVA+1.0 wt% rGO	55.200±1.060
PVA electrospun CVD-grown monolayer graphene	60.040±1.004

4.2.3. Optical Microscopy Analyses

The optical microscopy images of CVD-grown monolayer graphene at Cu foil, before and after peeling-off process (Cu foil only), were provided in Figure 5 with different magnifications. The grain boundaries of the CVD-grown monolayer graphene at Cu foil were easily seen in Figure 5 a-b. On the other hand, after the transfer of the graphene from Cu foil, no grain boundaries were observed on Cu foil anymore (Figure 5 c-d). Although, this phenomenon was also indicated by literature researchers [103], the other characterization studies were done to examine the quality of the transfer of the CVD-grown monolayer graphene, and the results were explained in the following sections.

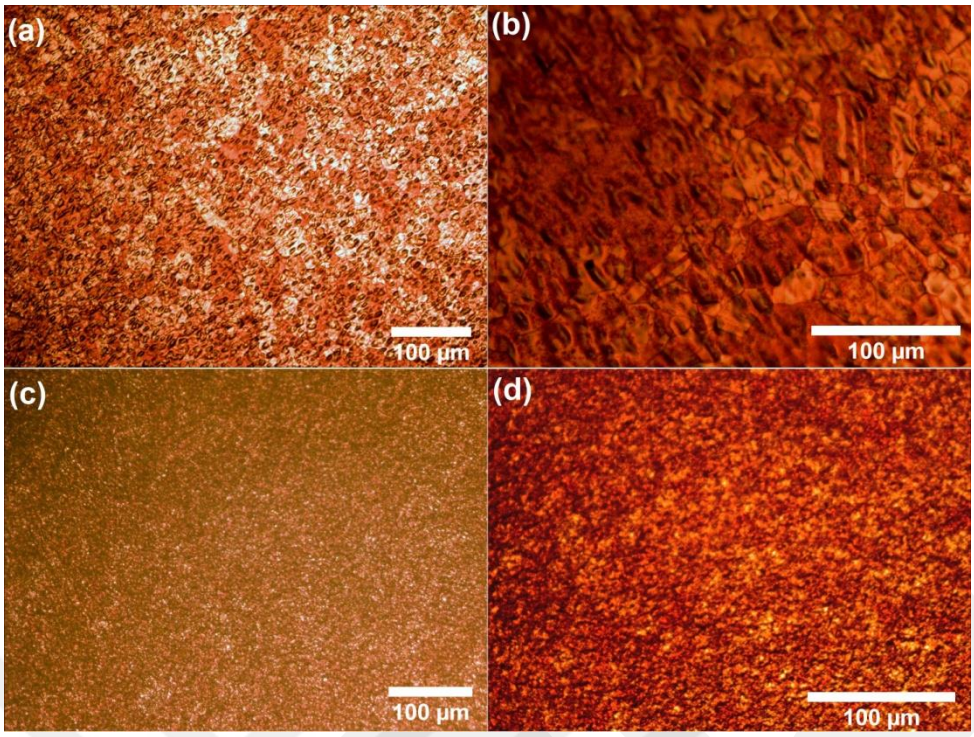

Figure 5. Optical microscopy images of CVD-grown monolayer graphene at Cu foil (a) x40, (b) x100; Cu foil only (c) x40, (d) x100.

4.2.4. Scanning Electron Microscope (SEM) Analyses

The fiber morphology of electrospun PVA mats, PVA+0.5 wt% rGO and PVA+1.0 wt% rGO nanocomposites was observed by SEM, and the images were provided in Figure 6. Besides, cross-sectional image of PVA+1.0 wt% rGO nanofibers was shown in Figure 6.f'. From the figure, it was seen that, continuous and bead-free nanofibers were obtained as a result of electrospinning process. Besides, it can be said that all electrospun structures had similar fiber characteristics with homogeneous fiber morphology.

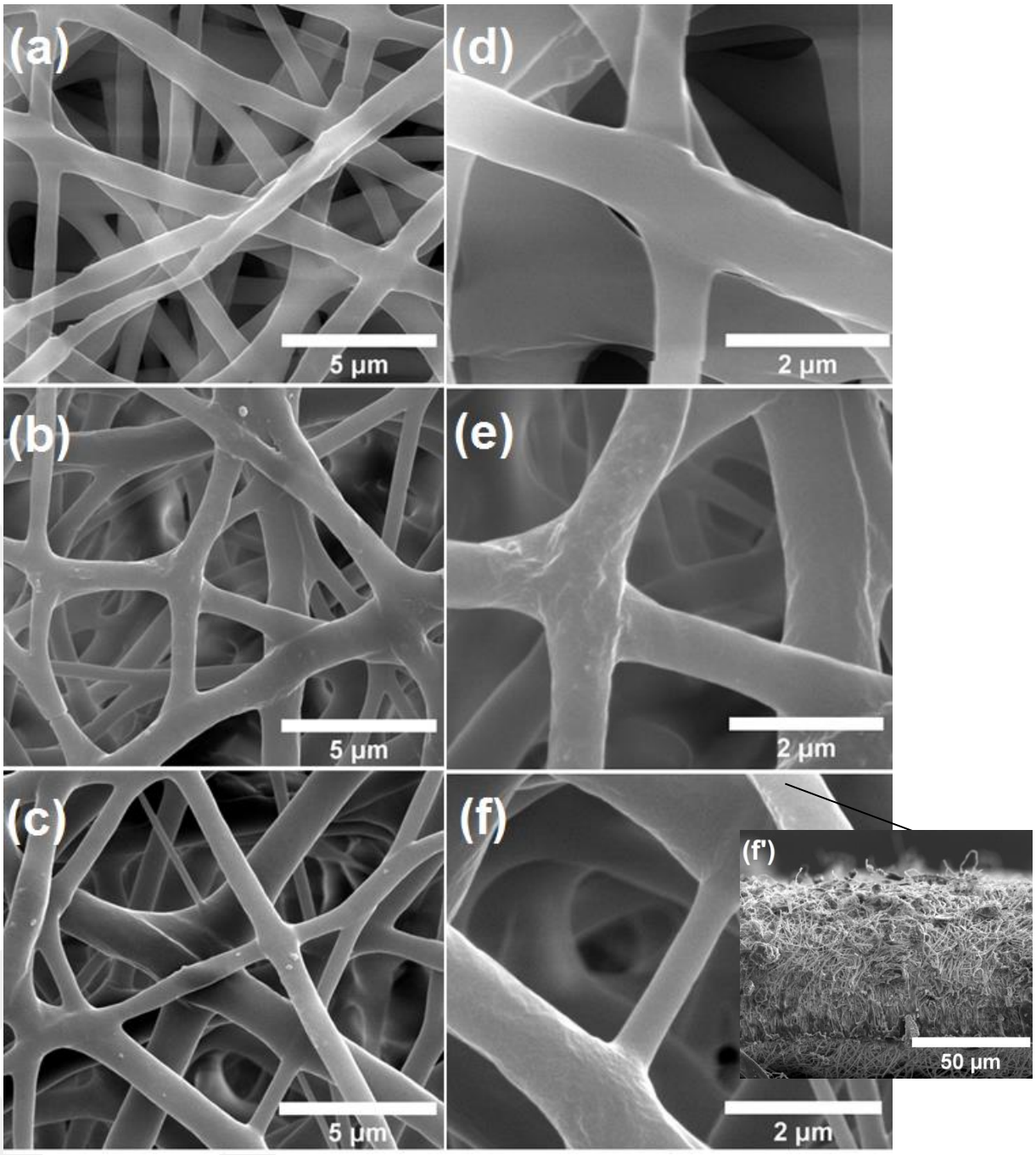

Figure 6. SEM images of electrospun a) PVA fibers, b) PVA+0.5 wt% rGO fibers and c) PVA+1.0 wt% rGO fibers x20000; d) PVA fibers, e) PVA+0.5 wt% rGO fibers and e) PVA+1.0 wt% rGO fibers x50000; f') cross-section of electrospun PVA+1.0 wt% rGO fibers x2500.

On the other hand, the transfer of graphene was examined with SEM in addition to the Optical Microscopy analyses and the images were provided in Figure 7 and 8. In Figure 7, it was observed that, after the transfer process, the grain boundaries of

CVD-grown monolayer graphene could not be seen at Cu foil, as it was expected. Moreover, the transfer of CVD-grown monolayer graphene from Cu foil to electrospun PVA mats with peeling-off procedure can be seen in Figure 8 due to the present graphene on the electrospun PVA mats. From the Figure 8, it was observed that graphene was partially transferred to the electrospun PVA.

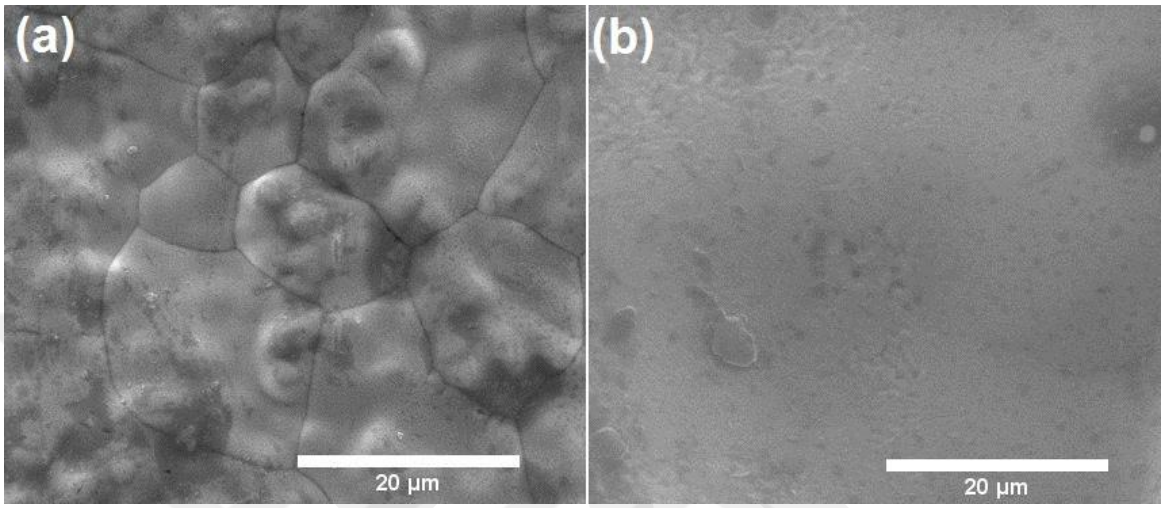

Figure 7. SEM images of (a) CVD-grown monolayer graphene at Cu foil, (b) Cu foil only, x5000.

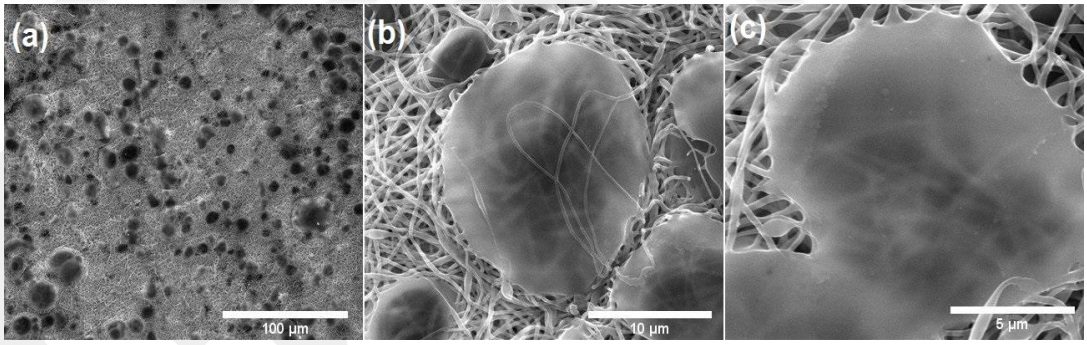

Figure 8. SEM images of PVA electrospun CVD-grown monolayer graphene nanocomposites (a) x1000, (b) x10000, (c) x20000.

4.2.5. Mechanical Properties

The tensile properties (elastic modulus, tensile strength and strain at break (%)) of the prepared electrospun PVA mats, PVA+0.5 wt% rGO and PVA+1.0 wt% rGO nanocomposites were determined and the obtained values were provided in Table 5. The control group, electrospun PVA mats, showed an elastic modulus of 1.210 MPa

and a tensile strength of 3.920 MPa which are typical values for an electrospun PVA [104]. The rGO added nanocomposites, on the other hand, showed improved elastic modulus and tensile strength values compared to the control group. The elastic modulus of electrospun PVA+0.5 wt% rGO was 1.410 MPa which was 116% (with 16% increment) and the tensile strength was 4.870 MPa which was 124%, of the control group. For the electrospun PVA+1.0 wt% rGO nanocomposites, the elastic modulus and tensile strength values were found as 1.490 MPa and 5.120 MPa, which were 123% and 130% of the control group, respectively. It was seen that, the addition of rGO enhanced the elastic modulus and tensile strength of the nanocomposites, and increment of rGO amount improved the elastic modulus as well as the tensile strength. Additionally, rGO added nanocomposites showed higher strain at break (%) values than that of control group. Electrospun PVA+1.0 wt% rGO nanocomposites had the highest strain at break (95%) value which showed more ductile properties resulting more elongation before failure. The tensile properties of PVA electrospun CVD-grown monolayer graphene nanocomposites were identical with those of electrospun PVA. All in all, rGO added nanocomposites exhibited improved tensile properties with an increase in ductility.

Table 5. Tensile properties of the nanocomposites.

Sample	**Elastic Modulus (GPa)**	**Tensile Strength (MPa)**	**Strain at Break (%)**
Electrospun PVA	1.210 ± 0.002	3.920 ± 0.010	88.200 ± 1.000
Electrospun PVA+0.5 wt% rGO	1.410 ± 0.025	4.870 ± 0.030	92.000 ± 0.960
Electrospun PVA+1.0 wt% rGO	1.490 ± 0.040	5.120 ± 0.040	95.010 ± 1.540
PVA electrospun CVD-grown monolayer graphene	1.210 ± 0.012	3.900 ± 0.010	88.100 ± 1.000

4.2.6. ATR-FTIR Analyses

FTIR spectroscopy is a sensitive and fast method to determine several chemical bonds and compositions in materials. The FTIR band of rGO, PVA mats, PVA+0.5 wt % rGO and PVA+1.0 wt % rGO nanocomposites were shown in Figure 9. In Fig. 9a, rGO showed typical absorption peaks at 3395, 1652, 1573 and 1387 cm^{-1} where they were associated with N-H stretching vibration, C=N bonds and C=C stretching respectively [72]. The COOH characteristic peaks are disappeared at about 1734 cm^{-1} (also the characteristic peaks of OH at 3430 cm^{-1} and the epoxy at 1050 cm^{-1} are disappeared) suggesting the majority of functional groups were removed from the surface of GO sheets in commercial rGO. In Figure 9b, the peaks presented in 2800-3000 cm^{-1} and 1200-1500 cm^{-1} represents the stretching and deformation vibrations of C-H groups of PVA [105]. Similarly, the vibrational bands at about 1750-1710 cm-1 of the spectrum of all the samples corresponded to C=O stretching of PVA (polymer) matrix [72,106]. Although there were no obvious changes in these ranges, there was a bond broadening at 2920 cm^{-1} in the PVA+0.5 wt % rGO and PVA+1.0 wt % rGO nanocomposites due to the C-H stretching of the polymer matrix [72]. In the literature, it was indicated that non-bonded -OH stretching bands are sensitive to the hydrogen bonding and the hydrogen bonded bands were found in the region of 3600-3000 cm^{-1} of Figure 9. From the spectra, it was clearly seen that the peak around 3408 cm^{-1} was shifted to a lower wavenumber with the addition of rGO, since the hydroxyl bands were found at 3339 cm^{-1} and 3301 cm^{-1} for PVA+0.5 wt % rGO and PVA+1.0 wt % rGO nanocomposites, respectively. This phenomenon has been observed for the assosication of the hydrogen bonding among the hydroxyl groups in PVA [72]. The results obtained from FTIR analyses showed that, a hydrogen bonding between PVA and rGO was exist, to the detriment of hydrogen bonding among PVA chains [72].

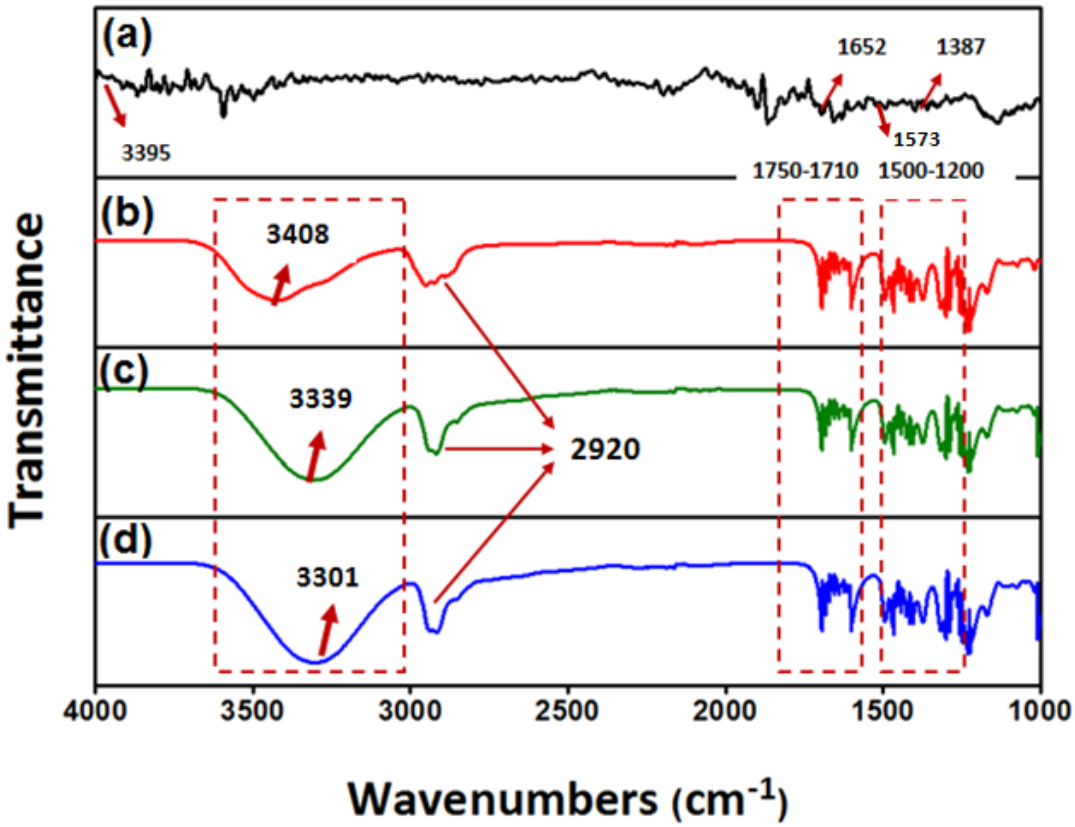

Figure 9. FTIR spectra of a) commercial rGO, electrospun b) PVA mats, c) PVA+0.5 wt % rGO and d) PVA+1.0 wt % rGO nanocomposites.

4.2.7. TGA Analyses

The TGA curves as a function of weight loss (%) of electrospun PVA mats, PVA+0.5 wt % rGO, PVA+1.0 wt % rGO and PVA electrospun CVD-grown monolayer graphene nanocomposites were shown in Figure 10. According to the obtained results, the temperature for the material decomposition within electrospun PVA mats was recorded as 345°C. When rGO was added to the PVA, it was seen that TGA curve was shifted to the higher temperature since the temperatures of decomposition for PVA+0.5 wt % rGO and PVA+1.0 wt % rGO nanocomposites were 20°C and 125 °C higher than that of control group, respectively. Besides, the decomposition temperature of PVA electrospun CVD-grown monolayer graphene nanocomposites was 100°C higher than the control group. On the other hand, the temperature of the maximum degradation rate was 450°C (obtained from the derivative of TGA curves) for PVA+1.0 wt % rGO nanocomposites, which is 140°C higher than that of control group (electrospun PVA mats). All of these results

obtained from the TGA analyses showed that, the decomposition behavior of the electrospun materials have been relatively improved because of the incorporation of graphene amount [107] and this phenomenon has been attributed to the physical barrier effect of graphene which slows down the diffusion, by other researchers in the literature [97].

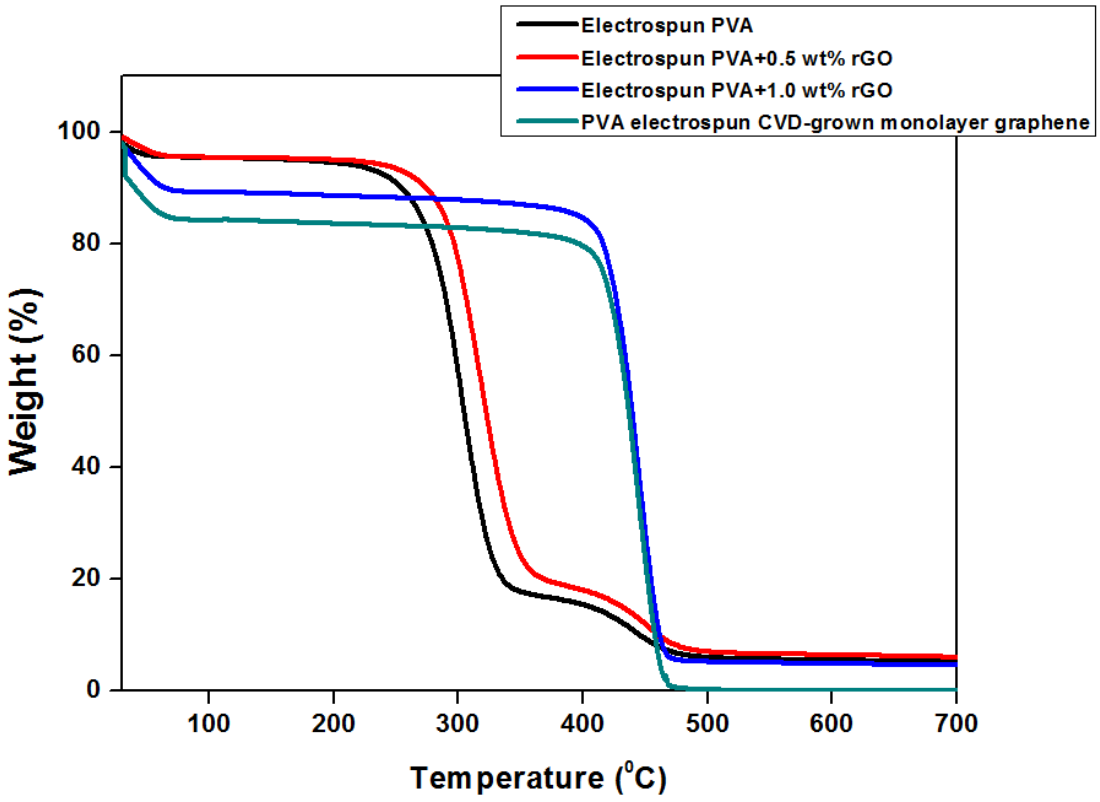

Figure 10. TGA curves of nanocomposites.

4.2.8. XRD Analyses

The XRD patterns of rGO, electrospun PVA mats, PVA+0.5 wt % rGO and PVA+1.0 wt % rGO nanocomposites were shown in Figure 11. In the spectra of rGO (Figure 11a), the sharp peak at 2Θ = 24° indicates the (002) plane corresponding the interlayer distance of 3.82 Å (d002) which is typical for graphitic structures. In the literature, it was reported that PVA is known as a semi crystalline polymer, thus it had a very intense peak in its XRD pattern at 2Θ = 19.6° which exhibits (101) diffraction peak [72]. For the electrospun PVA+0.5 wt % rGO nanocomposites, although the intense peak at 2Θ = 19.6° was a little bit wider, there

was no significant change of the peaks, when it was compared to the pattern of electrospun PVA mats. This situation was also observed for even higher amount of rGO addition to the PVA matrix (PVA+1.0 wt % rGO nanocomposites). When all these results were taken into consideration, it was concluded that rGO addition did not have any effect on the PVA crystallinity which indicates the complete and homogeneous dispersion of rGO. This similar phenomenon was also observed in the literature and the results obtained in this study were consistent with those indicated before [108].

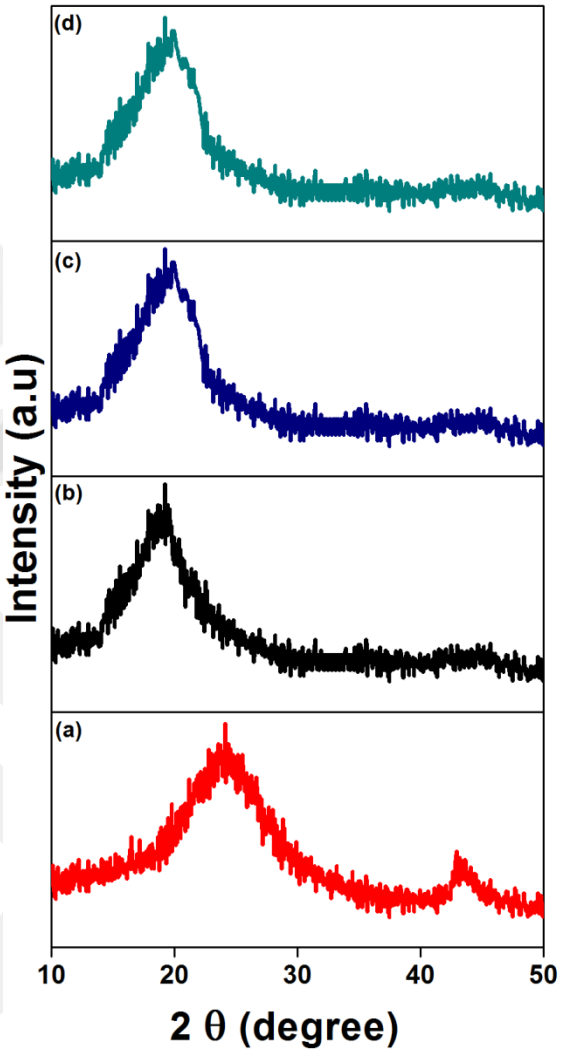

Figure 11. XRD patterns of a) commercial rGO, electrospun b) PVA mats, c) PVA+0.5 wt % rGO and d) PVA+1.0 wt % rGO nanocomposites.

4.2.9. Raman Analyses

Figure 12 showed the spectrum of electrospun PVA, neat CVD-grown monolayer graphene and PVA electrospun CVD-grown monolayer graphene as a result of Raman analyses. The most intense peak was seen at 2916 cm^{-1} for electrospun PVA due to the CH_2 stretching of the PVA chain [109]. Likewise, the peaks seen at 1173 and 1444 cm^{-1} were attributed to O-H and C-H vibrations of PVA, respectively [109]. On the other hand, in Figure 12b the G band represented the characteristics of graphitic crystalline structure at 1581 cm^{-1} and the characteristic 2D band was seen at and 2690 cm^{-1} [110]. In the Raman spectra of PVA electrospun CVD-grown monolayer graphene, the characteristic CH_2 stretching at 2916 cm^{-1}, the vibrations of O-H at 1172 and C-H at and 1444 cm^{-1} of PVA were also observed with less intensity. Similarly, the characteristic bands of graphene were found at 1581 (G) and 2690 (2D) cm^{-1} in the spectra. On the other hand, the I_G/I_{2D} ratio was calculated as 0.65 for the neat CVD-grown monolayer graphene where this ratio was 0.55 for PVA electrospun CVD-grown monolayer graphene. As a result, the presence of graphene on electrospun PVA structure was proved with Raman analyses.

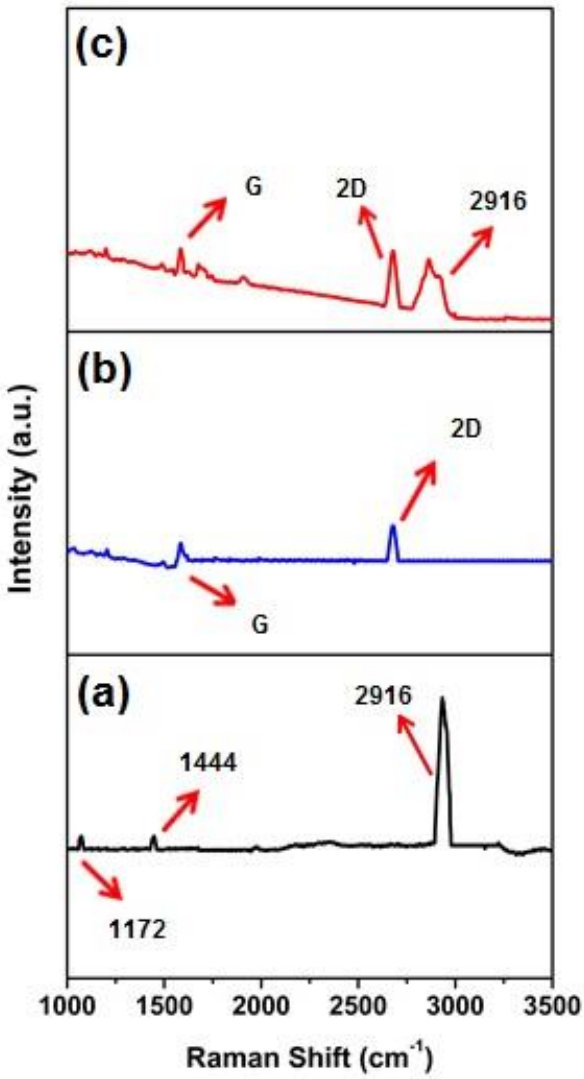

Figure 12. The raman spectra of a) electrospun PVA, b) neat CVD-grown monolayer graphene and c) PVA electrospun CVD-grown monolayer graphene.

4.2.10. PBS Absorption and Shrinkage Tests

The PBS absorption and shrinkage characteristics of the prepared samples were provided in Table 6. According to the table, it was seen that the lowest PBS absorption (%) value was measured for electrospun PVA (control group) mats (~80%) because of its relatively more hydrophobic structure among other samples. On the other hand, due to its more hydrophilic characteristics, the highest PBS absorption (%) value was measured for electrospun PVA+0.5 wt% rGO nanocomposites (~89%), followed by electrospun PVA+1.0 wt% rGO (~87%) and PVA electrospun CVD-grown monolayer graphene (~82%). This phenomenon was also seen for shrinkage (%) values, because the more absorption of PBS caused more

shrinkage due to the area change of the samples [111]. The results obtained from here were in consistency with the results obtained from CA measurements.

Table 6. PBS absorption (%) and shrinkage (%) values of the samples.

Sample	PBS Absorption (%)	Shrinkage (%)
Electrospun PVA	79.07 ± 2.4	4.1 ± 0.9
Electrospun PVA+0.5 wt% rGO	89.00 ± 0.9	5.1 ± 0.8
Electrospun PVA+1.0 wt% rGO	87.12 ± 1.1	4.6 ± 1.1
PVA electrospun CVD-grown monolayer graphene	82.05 ± 1.4	4.4 ± 0.6

4.2.11. In Vitro Degradation

In vitro degradation of the electrospun PVA mats, PVA+0.5 wt % rGO, PVA+1.0 wt % rGO and PVA electrospun CVD-grown monolayer graphene nanocomposites was presented in Figure 13 as a weight remaining graph, after degradation. In brief, the electrospun PVA had the slowest degradation rate because of the more hydrophobic character of it. Besides, electrospun PVA+0.5 wt% rGO mats had the fastest degradation rate among other sample groups, as it presented 100% weight loss after 72 days of the incubation followed by electrospun PVA+1.0 wt% rGO and PVA electrospun CVD-grown monolayer graphene nanocomposites. In fact, the electrospun PVA mats and PVA electrospun CVD-grown monolayer graphene nanocomposites had similar degradation behavior, as the major matrix was electrospun PVA for both of them. In the case of rGO added nanocomposites, it was seen that weight remaining is a little bit more for PVA+0.5 wt % rGO nanocomposites than PVA+1.0 wt % rGO nanocomposites till 30th day of the

incubation, however after 45 days of the incubation, it was observed that the degradation rate was faster for PVA+0.5 wt % rGO nanocomposites. This can be attributed to larger pore sizes of PVA+0.5 wt % rGO nanocomposites as the high network structures are willing to be exposed to lysozyme which increases degradation rates [111].

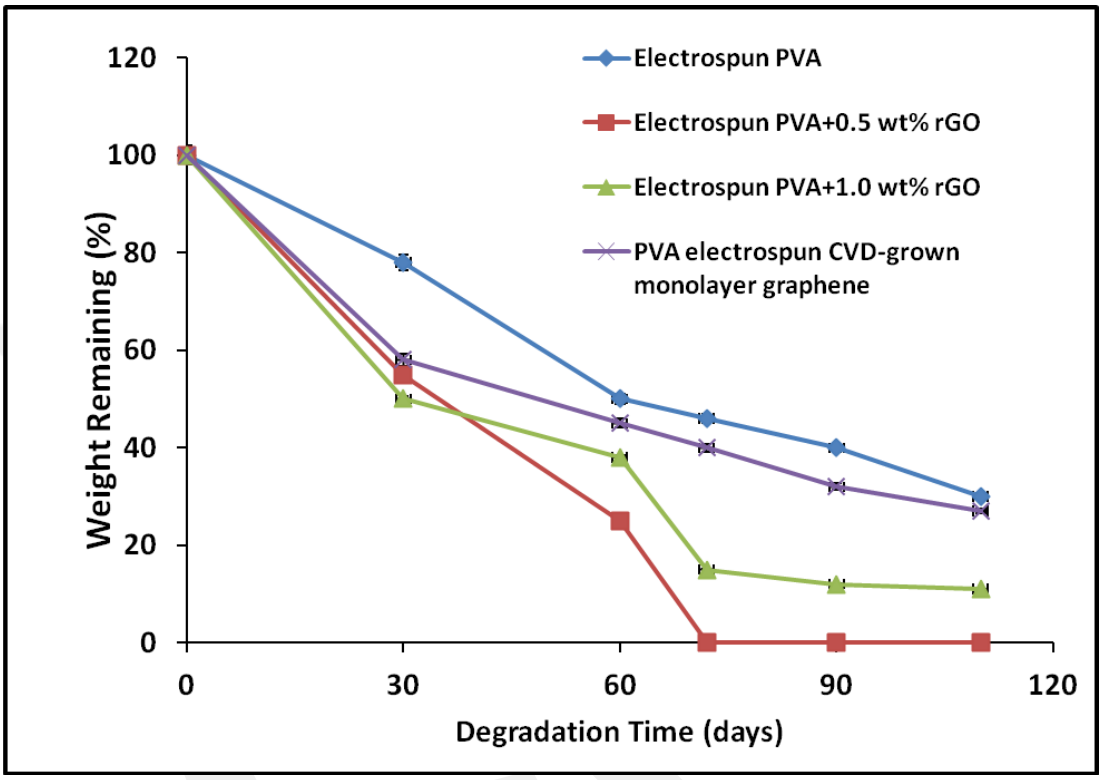

Figure 13. Weight remaining electrospun PVA mats, PVA+0.5 wt % rGO, PVA+1.0 wt % rGO and PVA electrospun CVD-grown monolayer graphene nanocomposites of as a function of degradation time.

4.2.12. WVTR

The WVTR of electrospun PVA mats, PVA+0.5 wt % rGO and PVA+1.0 wt % rGO were presented in Figure 14. It is known that WVTR depends on the surface wettability of a material, the porosity of fibers and the thickness of the mat. According to the WVTR results, the highest WVTR value was obtained for PVA+0.5 wt % rGO nanocomposites because of the enhanced hydrophilic character of it. Moreover, as reported before, WVTR increases with an increase in porosity of the fiber structure [98]. In the case of PVA+1.0 wt % rGO nanocomposites, it was seen that increase in conductivity of the solution, by the increased amount of rGO,

resulted lower fiber diameter (as discussed in Section 4.2.1), thus lower WVTR value was obtained.

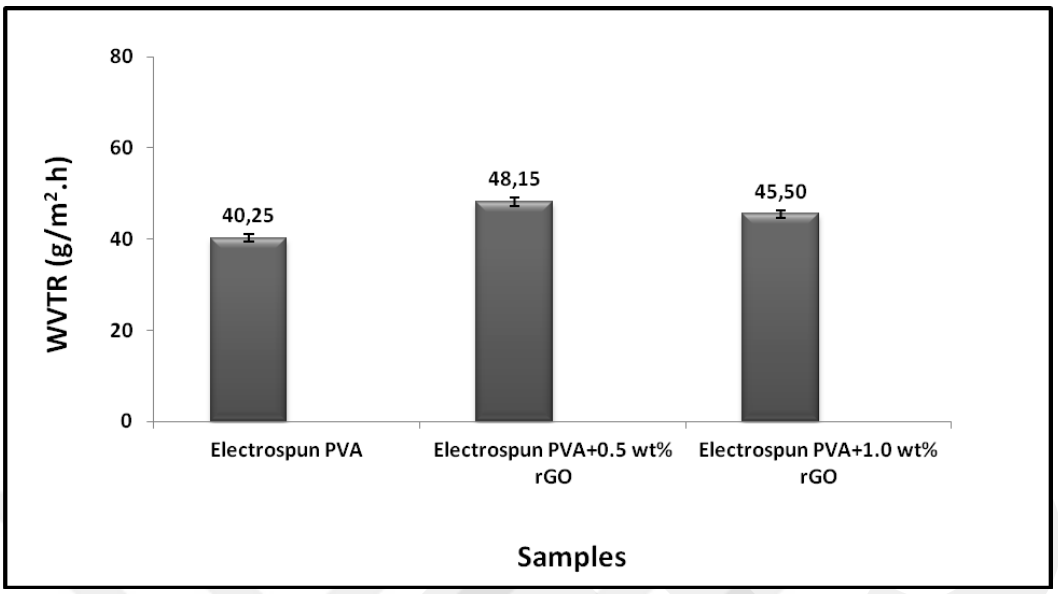

Figure 14. WVTR of electrospun PVA mats, PVA+0.5 wt % rGO and PVA+1.0 wt % rGO nanocomposites.

4.2.13. Electrical Conductivity Measurements

Electrical conductivities of the prepared nanocomposites were measured with a 4-point probe electrical conductivity device and the results were provided in Table 7. The most popular and common way of measuring the unknown resistivity (also conductivity) of a semiconductor material is to use a four-point collinear probe [112]. According to the Table 7, the lowest and the highest conductivities were measured for electrospun PVA and PVA+1.0 wt % rGO nanocomposites, respectively, as it was observed that an increase in rGO content increased the conductivity of the nanocomposites. This can be definitely attributed to the excellent electrical conductivity of rGO [113]. On the other hand, there was a slight increase in the electrical conductivity of PVA electrospun CVD-grown monolayer graphene nanocomposites. It was considered that partial location of graphene on the PVA mats and the domination of PVA amount along the matrix caused to obtain that value.

Table 7. Electrical conductivity of the nanocomposites.

Sample	Electrical Conductivity ($\mu S.cm^{-1}$)
Electrospun PVA	0.10±0.01
Electrospun PVA+0.5 wt% rGO	9.80±0.12
Electrospun PVA+1.0 wt% rGO	11.00±0.70
PVA electrospun CVD-grown monolayer graphene	0.40±0.21

4.3. Cell Culture Studies

4.3.1. MTT Assay

The tetrazolium salt, MTT, is widely used test method to measure cell viability and proliferation [114]. The viability of MG-63 cells on the prepared nanocomposites within 21 days was shown in Figure 15. The increased trend in the absorbance values with the increase in culture period indicated that the cells on all type of nanocomposites are willing to convert the MTT into formazan product and continue to proliferate during 21 days of incubation. At the end of the 21st day of cultivation period, the highest cell viability was observed for PVA+1.0 wt % rGO nanocomposites followed by the PVA+0.5 wt % rGO nanocomposites as the absorbance values increased proportional to the increased rGO content in the PVA matrix. On the other hand, the absorbance values for PVA electrospun CVD-grown monolayer graphene nanocomposites showed that cell viability was better than the control TCPS and electrospun PVA mats, however not as good as the electrospun rGO/PVA nanocomposites. This may be because of 2D structure of the monolayer graphene which is partially located on the surface of the electrospun structures. Besides, electrospun PVA had higher cell viability than the control TCPS due to its electrospun 3D structure. All in all, the MTT assay showed that graphene presence

(particularly rGO) on/within the nanocomposites support cell viability and this can be attributed to the enhanced electrical conductivity of the nanocomposites [115].

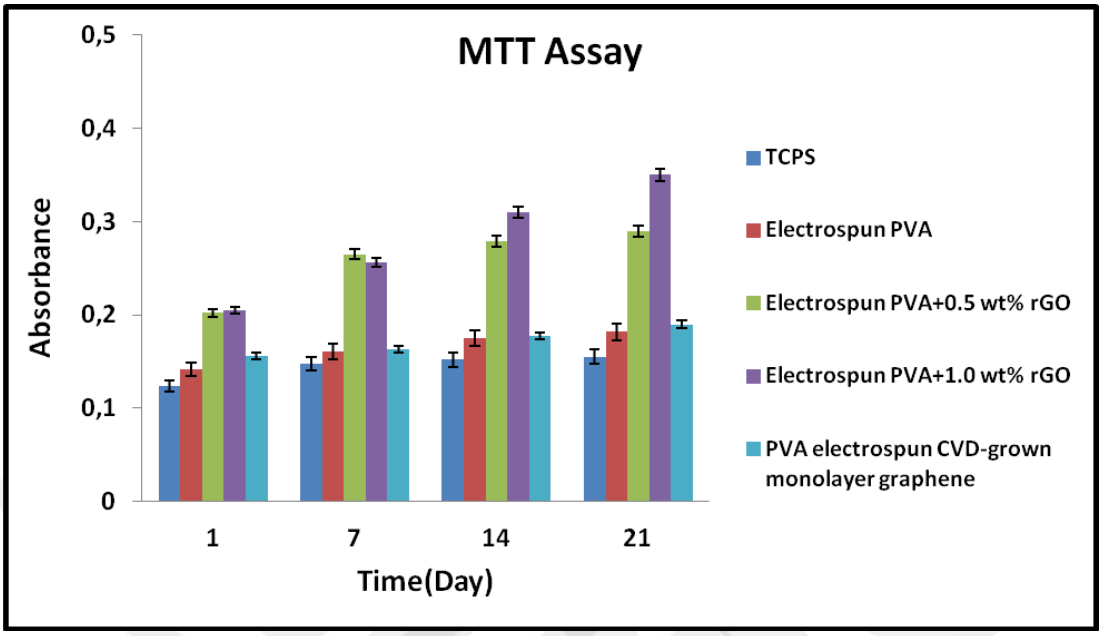

Figure 15. Absorbance values of the nanocomposites by MTT.

4.3.2. ALP Activity

ALP activity is an important marker for early osteoblastic differentiation which accumulates inorganic phosphate [116]. The results of the ALP activity of the MG-63 cells which cultured on electrospun PVA mats, PVA+0.5 wt % rGO, PVA+1.0 wt % rGO and PVA electrospun CVD-grown monolayer graphene nanocomposites were shown in Figure 16 as a (%) change after 7th, 14th and 21st day of the cultivation. It was observed that all types of electrospun nanocomposites supported cell proliferation, better than control TCPS during the culture period because of their 3D structure. The highest ALP activity was obtained for electrospun PVA+1.0 wt % rGO nanocomposites as it was expected and discussed in MTT assay studies attributed to enhanced electrical conductivities and tensile properties [115]. On the other hand, PVA electrospun CVD-grown monolayer graphene nanocomposites supported cell proliferation better than electrospun PVA and TCPS due to the partially located graphene on its surface. However, the ALP activity was not as high as those for rGO added nanocomposites because of the 2D structure of CVD-grown monolayer graphene. In the literature it was reported that 3D structures are willing to

support cell adhesion/proliferation better, thus these results obtained here were consistent with the MTT assay and literature [117].

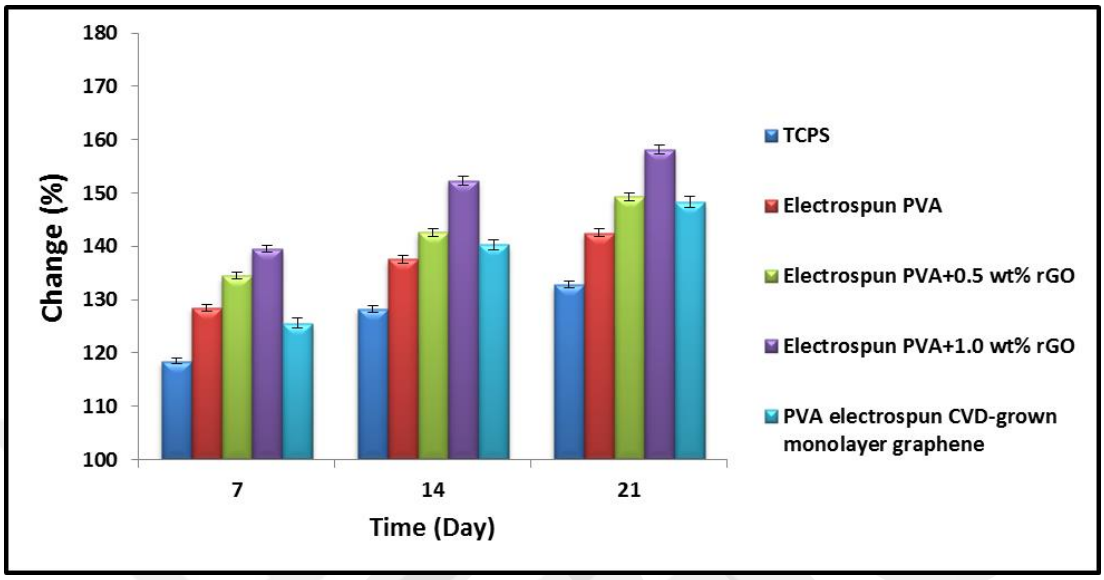

Figure 16. ALP activity of the MG-63 cells on the nanocomposites (BCIP tablet was used as blank substrate and its value was accepted as 100).

4.3.3. Alizarin Red Staining

To detect extracellular calcium deposits during the cultivation period, Alizarin Red Staining was performed for TCPS, electrospun PVA, PVA+0.5 wt % rGO, PVA+1.0 wt % rGO and PVA electrospun CVD-grown monolayer graphene nanocomposites on 7^{th}, 14^{th} and 21^{st} days of cultivation. The results were provided in Figure 17 and the color change as a result of Ca^{+2} could be seen in Figure 18. All types of electrospun samples showed better mineralization than the control TCPS due to their 3D structures [31]. The highest mineralization was detected in cells cultured on electrospun PVA+1.0 wt % rGO nanocomposites that stained the deepest red color compared to the other samples because of the enhanced biocompatible property of rGO. This result was consistent with those obtained by MTT Assay and ALP Activity studies. On the other hand, mineralization in the cells cultured on PVA electrospun CVD-grown monolayer graphene nanocomposites was higher than that of electrospun PVA mats due to the presence of CVD-grown monolayer graphene on the surface.

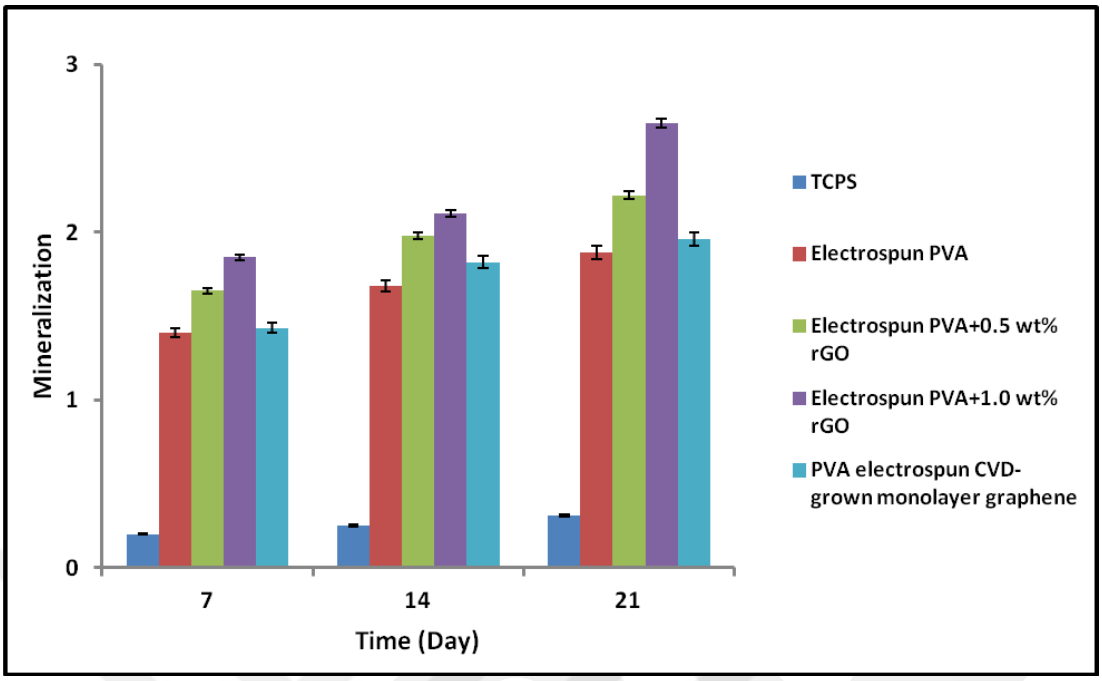

Figure 17. Quantification of MG-63 cell mineralization cultured on the nanocomposites.

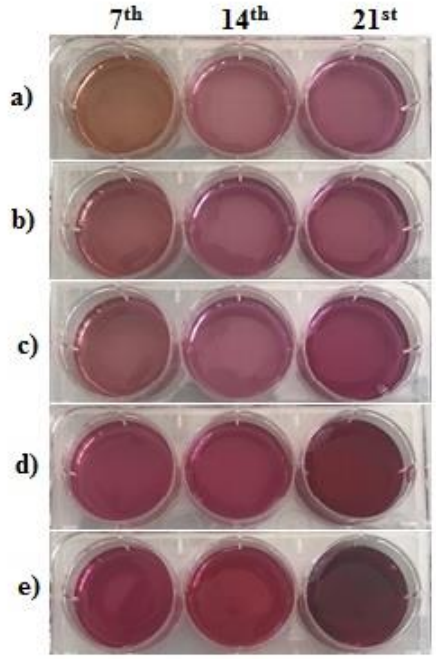

Figure 18. The color change as a result of Ca^{+2} deposition on a)TCPS, b) electrospun PVA, c) PVA electrospun CVD-grown monolayer graphene, d) PVA+0.5 wt % rGO, e) PVA+1.0 wt % rGO nanocomposites on 7^{th}, 14^{th} and 21^{st} days of cultivation.

4.3.4. Fluorescence Microscopy Analyses

The fluorescence microscopy analyses were performed to investigate cell viability, attachment and growth cultured on the prepared nanocomposites on 7th, 14th and 21st days of the cultivation and the images were provided in Figure 19. It was clearly observed that the cell attachment and viability were increased with the increase in culture period for all type of samples. On the other hand all electrospun structures had higher cell population than the control TCPS because of their 3D structures [31]. Besides, as it was expected from MTT Assay, ALP Activity and Alizarin Red Staining Tests, the highest cell viability, attachment and growth were obtained for electrospun PVA+1.0 wt % rGO nanocomposites. PVA electrospun CVD-grown monolayer graphene nanocomposites supported cell attachment and growth more than control TCPS and electrospun PVA mats. After all, it was concluded that graphene presence on/within the nanocomposites enhanced the biocompatible properties of them [115].

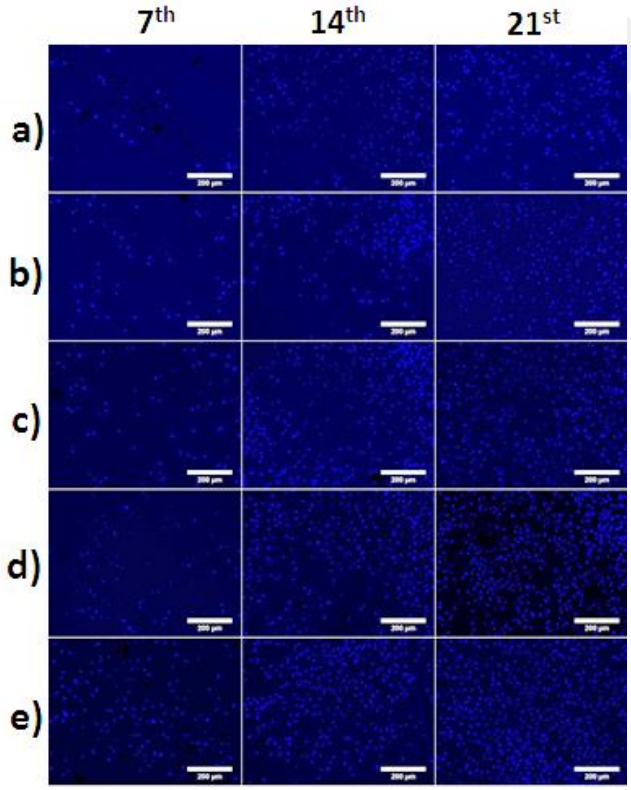

Figure 19. Flourescence images (by DAPI stain) a) TCPS, b) Electrospun PVA, c) CVD-grown monolayer graphene, d) Electrospun PVA+0.5 wt % rGO e) Electrospun PVA+1.0 wt % rGO nanocomposites, on 7th, 14th and 21st days of cultivation.

4.3.5. Observations with SEM

The cell morphology and attachment on the developed nanocomposites were examined with SEM on the 7th and 21st days of the cultivation. The images of electrospun PVA and PVA+1.0 wt % rGO were given in Figure 20. It was clearly seen that cell attachment was higher on the electrospun PVA+1.0 wt % rGO nanocomposites (Figure 20 a, b, d and e) as it was previously observed. Additionally, it was observed that cells kept their characteristic morphology during the culture for two types of samples (Figure 20 c and f).

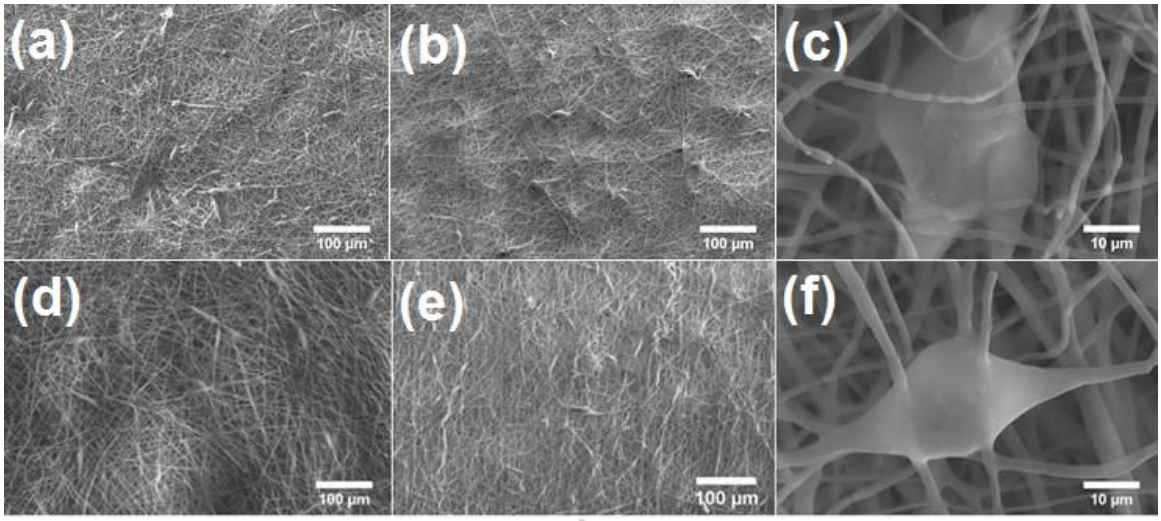

Figure 20. SEM images of MG-63 cells on/within electrospun PVA on a) 7th day, x500, b) 21st day, x500, c) 21st day, x10000; and electrospun PVA+1.0 wt % rGO nanocomposites d) 7th day, x500 e) 21st day, x500, f) 21st day, x10000.

CHAPTER 5

Conclusions

In this study, novel nanocomposites were developed with using PVA and forms of graphene by electrospinning and conclusions were given below.

- For the production of PVA mats and PVA+rGO nanocomposites, 2 g of PVA powder was dissolved in 30 ml distilled water and magnetically stirred at 90°C for 3 hours, and then rGO was added to the PVA mixtures and magnetically stirred for 5 hours with the concentration of rGO in the solution as 0.5 and 1.0 wt%. To prepare PVA mats, electrospinning parameters were found as; the distance between needle and the collector was 20 cm, voltage was 20 kV and the feeding rate 6.7 μL/min. For the PVA+0.5 wt % rGO nanocomposites, electrospinning parameters were determined as; the distance between needle and the collector was 6 cm, voltage was 22 kV and the feeding rate was 17 μL/min. Lastly, the distance between needle and the collector was 10 cm, voltage was 22 kV and the feeding rate was 15 μL/min were determined for PVA+1.0 wt % rGO nanocomposites.

- Complete crosslinking was seen for 75 min, 60 min and 45 min for electrospun PVA mats, PVA +0.5 wt % rGO and PVA+1.0 wt % rGO nanocomposites, respectively. They were remained stable both in the water and PBS solutions for more than 1 month.

- According to the measurements, the thicknesses of the prepared scaffolds were almost the same, in the range of 0.053-0.054 mm.

- The highest fiber diameter was measured as ~388 nm for electrospun PVA+0.5 wt% rGO nanocomposites whereas the lowest fiber diameter was measured as ~340 nm for the electrospun PVA mats because small amount of rGO addition moderated the viscosity hence increased the fiber diameter. However, increasing rGO content more, increased the electrical conductivity

of the precursor which caused a smaller fiber diameter (~365 nm) for electrospun PVA+1.0 wt % rGO nanocomposites.

- The highest porosity (%) was seen for electrospun PVA+0.5 wt % rGO nanocomposites (nearly the same, but a little more than PVA+1.0 wt % rGO nanocomposites) where the lowest porosity (%) was seen for electrospun PVA mats.

- The results obtained from CA measurements showed that crosslinked PVA had a ~62° surface wettability while CA could not be measured for non-crosslinked PVA. With the presence of rGO, lower CA values were obtained for the nanocomposites leading more hydrophilic structures due to the hydrophilic character of reduced graphene oxide owing functional O groups. On the other hand, the CA value of PVA electrospun CVD-grown monolayer graphene nanocomposites was measured as ~60° because of the moderate wettability characteristics of CVD-grown graphene.

- For PVA electrospun CVD-grown monolayer graphene nanocomposites, the optical microscopy analyses showed the transfer of graphene as the grain boundaries were not be observed after the peeling-off procedure.

- SEM analyses proved that continuous and bead-free nanofibers were obtained as a result of electrospinning process and all electrospun structures had similar fiber characteristics with homogeneous fiber morphology. On the other hand, SEM analyses showed that the transfer of graphene was completed partially.

- According to the mechanical property analyses, it was observed that rGO added nanocomposites exhibited improved tensile properties with an increase in ductility. Besides, it was observed that, the mechanical properties of PVA electrospun CVD grown monolayer graphene was identical with those of electrospun PVA mats as the main matrix was electrospun PVA.

- ATR-FTIR analyses showed that the peak around 3408 cm^{-1} was shifted to a lower wavenumber with the addition of rGO, because the hydroxyl bands were found at 3339 cm^{-1} and 3301 cm^{-1} for PVA+0.5 wt % rGO and PVA+1.0 wt % rGO nanocomposites, respectively, because of the

dissociation of the hydrogen bonding among the hydroxyl groups in PVA. Also, this analyses proved that a hydrogen bonding between PVA and rGO was exist which can be attributed to the detriment of hydrogen bonding among PVA chains.

- Through TGA analyses, it was seen that the decomposition behavior of the electrospun materials have been relatively improved because of the incorporation of graphene amount due to the physical barrier effect of graphene which slows down the diffusion.

- From XRD studies, it was concluded that 0.5 wt % and 1.0 wt % of rGO addition did not have any effect on the PVA crystallinity as a result of complete and homogeneous dispersion of rGO in the solution.

- The transfer of CVD grown monolayer graphene from Cu foil to electrospun PVA was proved with Raman analyses because the characteristics bands of graphene were found at 1173 and 1444 cm^{-1} of the sample spectra.

- The lowest PBS absorption (%) value was measured for electrospun PVA mats (~80%) because of its relatively more hydrophobic structure among other samples and due to its more hydrophilic characteristics, the highest PBS absorption (%) value was measured for electrospun PVA+0.5 wt% rGO nanocomposites (~89%), followed by electrospun PVA+1.0 wt% rGO (~87%) and PVA electrospun CVD-grown monolayer graphene (~82%).

- In vitro degradation studies indicated that electrospun PVA+0.5 wt% rGO mats had the fastest degradation rate because it has larger pore sizes and more hydrophilic character than other sample groups.

- Electrical conductivity measurements showed that an increase in rGO content in the polymer matrix increased the conductivity of the nanocomposites, while partially located graphene did not improved the conductivity as required.

- An increase in conductivity of the solution, by the increased amount of rGO, resulted lower fiber diameter, thus lower WVTR value was obtained.

- Cell culture studies performed by MTT Assay, ALP Activity, Alizarin Red Staining, Fluorescence Microscopy and SEM Analyses showed that electrospun PVA+1.0 wt% rGO nanocomposites were more biocompatible among other materials that have been studied in this thesis.

- All in all, at the end of all characterization studies it was suggested that electrospun PVA+1.0 wt% rGO nanocomposites were suitable candidates to be used in possible applications such as packaging, electrical, thermal and tissue engineering.

REFERENCES

1. L. Khandare and D. Late, "MoO_3-rGO nanocomposites for electrochemical energy storage", Applied Surface Science 418 (2017) 2-8.

2. M. Zakaria, M. Abdul Kudus, H. Md. Akil and M. Mohd Thirmizir, "Comparative study of graphene nanoparticle and multiwall carbon nanotube filled epoxy nanocomposites based on mechanical, thermal and dielectric properties", Composites Part B: Engineering 119 (2017) 57-66.

3. J. Jordan, K. Jacob, R. Tannenbaum, M. Sharaf and I. Jasiuk, "Experimental trends in polymer nanocomposites-a review", Materials Science and Engineering: A 393 1-2 (2005) 1-11.

4. S.A. Zavyalov, A.N. Pivkina and J. Schoonman, Solid State Ionics 147 (2002) 415–419.

5. R. Bogue, "Nanocomposites: a review of technology and applications", Assembly Automation 31:2 (2011) 106-112.

6. S. Saber-Samandari and S. Saber-Samandari, "Biocompatible nanocomposite scaffolds based on copolymer-grafted chitosan for bone tissue engineering with drug delivery capability", Materials Science and Engineering: C 75 (2017) 721-732.

7. M. Naeimi, M. Rafienia, M. Fathi, M. Janmaleki, S. Bonakdar and M. Ebrahimian Hosseinabadi, “Incorporation of chitosan nanoparticles into silk fibroin-based porous scaffolds: Chondrogenic differentiation of stem cells, International Journal of Polymeric Materials and Polymeric Biomaterials 65 (2016) 202–209.

8. Y. Zare and K. Rhee, "Development of a conventional model to predict the electrical conductivity of polymer/carbon nanotubes nanocomposites by interphase, waviness and contact effects", Composites Part A: Applied Science and Manufacturing 100 (2017) 305-312.

9. B. Yang, J. Jang, S. Eem and S. Kim, "A probabilistic micromechanical modeling for electrical properties of nanocomposites with multi-walled carbon nanotube morphology", Composites Part A: Applied Science and Manufacturin. 92 (2017) 108-117.

10. H. Sasmazel and O. Ozkan, "Advances in Electrospinning of Nanofibers and their Biomedical Applications", Current Tissue Engineering 2:2 (2013) 91-108.

11. V. Beachley and X. Wen, "Polymer nanofibrous structures: Fabrication, biofunctionalization, and cell interactions", Progress in Polymer Science 35:7 (2010) 868-892.

12. B. Ouadil, O. Cherkaoui, M. Safi and M. Zahouily, "Surface modification of knit polyester fabric for mechanical, electrical and UV protection properties by coating with graphene oxide, graphene and graphene/silver nanocomposites", Applied Surface Science 414 (2017) 292-302.

13. Z. Li and Y. Wang, "Preparation of polymer-derived graphene-like carbon-silicon carbide nanocomposites as electromagnetic interference shielding material for high temperature applications", Journal of Alloys and Compounds 709 (2017) 313-321.

14. L. Fan, H. Yang, J. Yang, M. Peng and J. Hu, "Preparation and characterization of chitosan/gelatin/PVA hydrogel for wound dressings", Carbohydrate Polymers 146 (2017) 427-434.

15. L. Xia, C. Li and Y. Wang, "In-situ crosslinked PVA/organosilica hybrid membranes for pervaporation separations", Journal of Membrane Science 498 (2017) 263-275.

16. W. Choi, I. Lahiri, R. Seelaboyina and Y. Kang, "Synthesis of Graphene and Its Applications: A Review", Critical Reviews in Solid State and Materials Sciences, 35:1 (2017) 52-71.

17. M. Acik and Y. Chabal, "A Review on Reducing Graphene Oxide for Band Gap Engineering", Journal of Materials Science Research 2:1 (2012) 101-112.

18. N. Pal, P. Dubey, P. Gopinath and K. Pal, "Combined effect of cellulose nanocrystal and reduced graphene oxide into poly-lactic acid matrix nanocomposite as a scaffold and its anti-bacterial activity", International Journal of Biological Macromolecules 95 (2017) 94-105

19. D. Ma, Y. Zhang, M. Gao, Y. Xin, J. Wu and N. Bao, "RGO/InVO4 hollowed-out nanofibers: Electrospinning synthesis and its application in photocatalysis", Applied Surface Science 353 (2017) 118-126.

20. M. Kalbac, O. Frank, L. Kavan, "The control of graphene double-layer formationin copper-catalyzed chemical vapor deposition", Carbon 50:10 (2012) 3682–3687.

21. Y. Zhao, X. Li, X. Zhou and Y. Zhang, "Review on the graphene based optical fiber chemical and biological sensors", Sensors and Actuators B 231 (2016) 324-340.

22. P. Camargo, K. Satyanarayana and F. Wypych, "Nanocomposites: synthesis, structure, properties and new application opportunities", Materials Research 12:1 (2009) 1-39.

23. K. Kumar, "Porous nanocomposites as catalyst supports", Applied Catalysis A: General 119:1 (1994) 163-183.

24. R. Mezzenga and J. Ruokolainen, "Nanocomposites: Nanoparticles in the right place", Nature Materials 8:12 (2009) 926-928.

25. R. Casati and M. Vedani, "Metal Matrix Composites Reinforced by Nano-Particles-A Review", Metals 4:1 (2014) 65-83.

26. S. Imani Yengejeh, S. Kazemi and A. Öchsner, "Carbon nanotubes as reinforcement in composites: A review of the analytical, numerical and experimental approaches", Computational Materials Science 136 (2017) 85-101.

27. J. Zhang and X. Peng, "Superior interfacial mechanical properties of boron nitride-carbon nanotube reinforced nanocomposites: A molecular dynamics study", Materials Chemistry and Physics 198 (2017) 250-257.

28. Y. Wang, L. Wang, F. An, H. Xu, Z. Yin, S. Tang, H. Yang and H. Song, "Graphitic carbon nitride supported platinum nanocomposites for rapid and sensitive colorimetric detection of mercury ions", Analytica Chimica Acta 980 (2017) 72-78.

29. Y. Zare, M. Fasihi and K. Rhee, "Efficiency of stress transfer between polymer matrix and nanoplatelets in clay/polymer nanocomposites", Applied Clay Science 143 (2017) 265-272.

30. A. Monfared and A. Jalali-Arani, "Morphology and rheology of (styrene-butadiene rubber/acrylonitrile-butadiene rubber) blends filled with organoclay: The effect of nanoparticle localization", Applied Clay Science 108 (2015) 1-11.

31. H. Sasmazel, "Novel hybrid scaffolds for the cultivation of osteoblast cells", International Journal of Biological Macromolecules 49:4 (2011) 838-846.

32. S. Jana and K. Sen, "Chitosan - Locust bean gum interpenetrating polymeric network nanocomposites for delivery of aceclofenac", International Journal of Biological Macromolecules 102 (2017) 878-884.

33. K. Narayanan and S. Han, "Dual-crosslinked poly(vinyl alcohol)/sodium alginate/silver nanocomposite beads – A promising antimicrobial material", Food Chemistry 234 (2017) 103-110.

34. V. Raj and G. Prabha, "Synthesis, characterization and in vitro drug release of cisplatin loaded Cassava starch acetate–PEG/gelatin nanocomposites", Journal of the Association of Arab Universities for Basic and Applied Sciences 21 (2016) 10-16.

35. M. Barmouz and A. Behravesh, "Statistical and experimental investigation on low density microcellular foaming of PLA-TPU/cellulose nano-fiber bio-nanocomposites", Polymer Testing 61 (2017) 300-313.

36. I. Donald and P. McMillan, "Ceramic-matrix composites", Journal of Materials Science 11:5 (1976) 949-972.

37. N. Selvakumar, M. Jinnah Sheik Mohamed, R. Narayanasamy and K. Venkateswarlu, "Forming limit diagram and void coalescence analyses of AA5052 coated with molybdenum-based ceramic nanocomposites", Materials & Design (1980-2015) 52 (2013) 393-403.

38. J. Njuguna and K. Pielichowski, "Polymer Nanocomposites for Aerospace Applications: Properties", Advanced Engineering Materials 5:11 (2003) 769-778.

39. B. Cristina, D. Ion, S. Adriana and P. George, "Nanocomposites as Advanced Materials for Aerospace Industry", INCAS BULLETIN 4:4, (2012) 57-72.

40. E. Siochi and J. Harrison, "Structural nanocomposites for aerospace applications", MRS Bulletin 40:10 (2015) 829-835.

41. S. Maisanaba, N. Ortuño, M. Jordá-Beneyto, S. Aucejo and Á. Jos, "Development, characterization and cytotoxicity of novel silane-modified clay minerals and nanocomposites intended for food packaging", Applied Clay Science 138 (2017) 40-47.

42. K. Ng, G. Tan and S. Khor, "Graphite nanocomposites sensor for multiplex detection of antioxidants in food", Food Chemistry 237 (2017) 912-920.

43. L. Xiao-e, A. Green, S. Haque, A. Mills and J. Durrant, "Light-driven oxygen scavenging by titania/polymer nanocomposite films", Journal of Photochemistry and Photobiology A: Chemistry 162:2-3 (2004)2 53-259.

44. L. Qi, Z. Xu, X. Jiang, C. Hu and X. Zou, "Preparation and antibacterial activity of chitosan nanoparticles", Carbohydrate Research 339 16 (2004) 2693-2700.

45. S. Ray, S. Quek, A. Easteal and X. Chen, "The Potential Use of Polymer-Clay Nanocomposites in Food Packaging", International Journal of Food Engineering 2: 4 (2006).

46. J. Rhim and P. Ng, "Natural Biopolymer-Based Nanocomposite Films for Packaging Applications", Critical Reviews in Food Science and Nutrition 47:4 (2007) 411-433.

47. M. Gao, L. Lu, X. Xu, Z. Yao and Y. Jiang, “Electropolymerization and multifunctional properties of novel polypyrrole films embedded with Co nanoparticles”, Electrochimica Acta 228 (2017) 522-527.

48. A. Khalil, M. Hassan and A. Ward, "Novel nanofibrillated cellulose/polyvinylpyrrolidone/silver nanoparticles films with electrical conductivity properties", Carbohydrate Polymers 157 (2017) 503-511.

49. H. Ju and J. Kim, "Fabrication of conductive polymer/inorganic nanoparticles composite films: PEDOT:PSS with exfoliated tin selenide nanosheets for polymer-based thermoelectric devices", Chemical Engineering Journal 297 (2016) 66-73.

50. K. Gómez-Lizárraga, C. Flores-Morales, M. Del Prado-Audelo, M. Álvarez-Pérez, M. Piña-Barba and C. Escobedo, "Polycaprolactone- and

polycaprolactone/ceramic-based 3D-bioplotted porous scaffolds for bone regeneration: A comparative study", Materials Science and Engineering: C 79 (2017) 326-335.

51. R. Huang, X. Zhu, H. Tu and A. Wan, "The crystallization behavior of porous poly(lactic acid) prepared by modified solvent casting/particulate leaching technique for potential use of tissue engineering scaffold", Materials Letters 136 (2014) 126-129.

52. M. Gozutok, A. Baitukha, F. Arefi-Khonsari and H. Turkoglu Sasmazel, "Novel thin films deposited on electrospun PCL scaffolds by atmospheric pressure plasma jet for L929 fibroblast cell cultivation", Journal of Physics D: Applied Physics 49:47 (2016) 474002.

53. D. Ronca, F. Langella, M. Chierchia, U. D'Amora, T. Russo, M. Domingos, A. Gloria, P. Bartolo and L. Ambrosio, "Bone Tissue Engineering: 3D PCL-based Nanocomposite Scaffolds with Tailored Properties", Procedia CIRP 49 (2016) 51-54.

54. O. Ozkan and H. Sasmazel, "Hybrid Polymeric Scaffolds Prepared by Micro and Macro Approaches", International Journal of Polymeric Materials and Polymeric Biomaterials (2017).

55. A. Marino, C. Tonda-Turo, D. De Pasquale, F. Ruini, G. Genchi, S. Nitti, V. Cappello, M. Gemmi, V. Mattoli, G. Ciardelli and G. Ciofani, "Gelatin/nanoceria nanocomposite fibers as antioxidant scaffolds for neuronal regeneration", Biochimica et Biophysica Acta (BBA) - General Subjects 1861:2 (2017) 386-395.

56. A. El-Kady, R. Rizk, B. Abd El-Hady, M. Shafaa and M. Ahmed, "Characterization, and antibacterial properties of novel silver releasing nanocomposite scaffolds fabricated by the gas foaming/salt-leaching technique", Journal of Genetic Engineering and Biotechnology 10:2 (2012) 229-238.

57. C. Zhang, X. Yuan, L. Wu, Y. Han and J. Sheng, "Study on morphology of electrospun poly(vinyl alcohol) mats", European Polymer Journal 41:3 (2005) 423-432.

58. G. Eda and S. Shivkumar, "Bead-to-fiber transition in electrospun polystyrene", Journal of Applied Polymer Science 106:1 (2007) 475-487.

59. Y. Zhao, Q. Yang, X. Lu, C. Wang and Y. Wei, "Study on correlation of morphology of electrospun products of polyacrylamide with ultrahigh molecular weight", Journal of Polymer Science Part B: Polymer Physics 43:16 (2005) 2190-2195.

60. S. Sukigara, M. Gandhi, J. Ayutsede, M. Micklus and F. Ko, "Regeneration of Bombyx mori silk by electrospinning-part 1: processing parameters and geometric properties", Polymer, vol. 44, no. 19, pp. 5721-5727, 2003.

61. X. Zong, K. Kim, D. Fang, S. Ran, B. Hsiao and B. Chu, "Structure and process relationship of electrospun bioabsorbable nanofiber membranes", Polymer 43:16 (2002) 4403-4412.

62. D. Reneker and I. Chun, "Nanometre diameter fibres of polymer, produced by electrospinning", Nanotechnology 7:3 (1996) 216-223.

63. M. Demir, I. Yilgor, E. Yilgor and B. Erman, "Electrospinning of polyurethane fibers", Polymer 43:11 (2002) 3303-3309.

64. B. Ding, H. Kim, S. Lee, C. Shao, D. Lee, S. Park, G. Kwag and K. Choi, "Preparation and characterization of a nanoscale poly(vinyl alcohol) fiber aggregate produced by an electrospinning method", Journal of Polymer Science Part B: Polymer Physics 40:13 (2002) 1261-1268.

65. C. Buchko, L. Chen, Y. Shen and D. Martin, "Processing and microstructural characterization of porous biocompatible protein polymer thin films", Polymer 40:26 (1999) 7397-7407.

66. C. Mit-uppatham, M. Nithitanakul and P. Supaphol, "Ultrafine Electrospun Polyamide-6 Fibers: Effect of Solution Conditions on Morphology and Average Fiber Diameter", Macromolecular Chemistry and Physics 205:17 (2004) 2327-2338.

67. C. Casper, J. Stephens, N. Tassi, D. Chase and J. Rabolt, "Controlling Surface Morphology of Electrospun Polystyrene Fibers: Effect of Humidity and Molecular Weight in the Electrospinning Process", Macromolecules 37:2 (2004) 573-578.

68. L. Carnell, E. Siochi, N. Holloway, R. Stephens, C. Rhim, L. Niklason and R. Clark, "Aligned Mats from Electrospun Single Fibers", Macromolecules 41:14 (2008) 5345-5349.

69. L. Chen, L. Bromberg, T. Hatton and G. Rutledge, "Catalytic hydrolysis of p-nitrophenyl acetate by electrospun polyacrylamidoxime nanofibers", Polymer 48:16, (2007) 4675-4682.

70. B. Ding, J. Kim, Y. Miyazaki and S. Shiratori, "Electrospun nanofibrous membranes coated quartz crystal microbalance as gas sensor for NH_3 detection", Sensors and Actuators B: Chemical 101 (2004) 373-380.

71. S. Wang, Y. Zhang, G. Yin, H. Wang and Z. Dong, "Fabrication of a composite vascular scaffold using electrospinning technology", Materials Science and Engineering: C 30:5 (2010) 670-676.

72. S. Kashyap, S. Pratihar and S. Behera, "Strong and ductile graphene oxide reinforced PVA nanocomposites", Journal of Alloys and Compounds 684 (2016) 254-260.

73. Z. Zarekhalili, S. Bahrami, M. Ranjbar-Mohammadi and P. Milan, "Fabrication and characterization of PVA/Gum tragacanth/PCL hybrid nanofibrous scaffolds for skin substitutes", International Journal of Biological Macromolecules 94 (2017) 679-690.

74. M. Ye, P. Mohanty and G. Ghosh, "Biomimetic apatite-coated porous PVA scaffolds promote the growth of breast cancer cells", Materials Science and Engineering: C 44 (2014) 310-316.

75. P. Vashisth, K. Nikhil, P. Roy, P. Pruthi, R. Singh and V. Pruthi, "A novel gellan-PVA nanofibrous scaffold for skin tissue regeneration: Fabrication and characterization", Carbohydrate Polymers 136 (2016) 851-859.

76. A. Esmaeili and A. Beni, "A novel fixed-bed reactor design incorporating an electrospun PVA/chitosan nanofiber membrane", Journal of Hazardous Materials 280 (2014) 788-796.

77. Y. Liu, R. Wang, H. Ma, B. Hsiao and B. Chu, "High-flux microfiltration filters based on electrospun polyvinylalcohol nanofibrous membranes", Polymer 54:2 (2013) 548-556.

78. J. Li, L. Shao, L. Yuan and Y. Wang, "A novel strategy for making poly(vinyl alcohol)/reduced graphite oxide nanocomposites by solvothermal reduction", Materials & Design (1980-2015) 54 (2014) 520-525.

79. M. El Achaby and A. Qaiss, "Processing and properties of polyethylene reinforced by graphene nanosheets and carbon nanotubes", Materials & Design 44 (2013) 81-89.

80. F. Xiao, Y. Li, X. Zan, K. Liao, R. Xu and H. Duan, “Growth of metal–metal oxide nanostructures on freestanding graphene paper for flexible biosensors”, Advanced Functional Materials 22 (2012) 2487–2494.

81. D. Bitounis, H. Ali-Boucetta, B. Hong, D. Min and K. Kostarelos, Prospects and challenges of graphene in biomedical applications, Advanced Materials 25 (2013) 2258–2268.

82. H. Pant, C. Park, L. Tijing, A. Amarjargal, D. Lee and C. Kim, “Bimodal fiber diameter distributed graphene oxide/nylon-6 composite nanofibrous

mats via electrospinning", Colloids and Surfaces:A Physicochemical and Engineering Aspects 407 (2012) 121–125.

83. S. Liu, T. Zeng, M. Hofmann, E. Burcombe, J. Wei, R. Jiang, J. Kong and Y. Chen, "Antibacterial Activity of Graphite, Graphite Oxide, Graphene Oxide, and Reduced Graphene Oxide: Membrane and Oxidative Stress", ACS Nano 5:9 (2011) 6971-6980.

84. S. Aznar-Cervantes, J. Martínez, A. Bernabeu-Esclapez, A. Lozano-Pérez, L. Meseguer-Olmo, T. Otero and J. Cenis, "Fabrication of electrospun silk fibroin scaffolds coated with graphene oxide and reduced graphene for applications in biomedicine", Bioelectrochemistry 108 (2016) 36-45.

85. K. Babu and W. Choi, "Thermal actuation properties of bimorph based on PVDF/rGO composites", Composites Science and Technology 122 (2016) 82-89.

86. Q. Ji, L. Shi, Q. Zhang, W. Wang, H. Zheng, Y. Zhang, Y. Liu and J. Sun, "VOx effectively doping CVD-graphene for transparent conductive films", Applied Surface Science 387 (2016) 51-57.

87. R. Jaaniso, T. Kahro, J. Kozlova, J. Aarik, L. Aarik, H. Alles, A. Floren, A. Gerst, A. Kasikov, A. Niilisk and V. Sammelselg, "Temperature induced inversion of oxygen response in CVD graphene on SiO_2", Sensors and Actuators B: Chemical 190 (2014) 1006-1013.

88. J. Fowler, M. Allen, V. Tung, Y. Yang, R. Kaner and B. Weiller, "Practical Chemical Sensors from Chemically Derived Graphene", ACS Nano 3:2 (2009) 301-306.

89. M. Gautam and A. Jayatissa, "Gas sensing properties of graphene synthesized by chemical vapor deposition", Materials Science and Engineering: C 31:7 (2011) 1405-1411.

90. X. Dong, Y. Shi, W. Huang, P. Chen and L. Li, "Electrical Detection of DNA Hybridization with Single-Base Specificity Using Transistors Based on CVD-Grown Graphene Sheets", Advanced Materials 22:14 (2010) 1649-1653.

91. H. Xie, M. Chua, I. Islam, R. Bentini, T. Cao, J. Viana-Gomes, A. Castro Neto and V. Rosa, "CVD-grown monolayer graphene induces osteogenic but not odontoblastic differentiation of dental pulp stem cells", Dental Materials 33:1 (2017) e13-e21.

92. Y. Kwak, D. Choi, Y. Kim, H. Kim, D. Yoon, S. Ahn, J. Yang, W. Yang and S. Seo, "Flexible glucose sensor using CVD-grown graphene-based field effect transistor", Biosensors and Bioelectronics 37:1 (2012) 82-87.

93. O. Rezaee, H. Mahmoudi Chenari, F. Ghodsi and H. Ziyadi, "Preparation of PVA nanofibers containing tungsten oxide nanoparticle by electrospinning and consideration of their structural properties and photocatalytic activity", Journal of Alloys and Compounds 690 (2017) 864-872.

94. P. Vashisth and V. Pruthi, "Synthesis and characterization of crosslinked gellan/PVA nanofibers for tissue engineering application", Materials Science and Engineering: C 67 (2016) 304-312.

95. Annual Book of ASTM Standards, ASTM F 1635-04: Standard Test Method for in vitro Degradation Testing of Hydrolytically Degradable Polymer Resins and Fabricated Forms for Surgical Implants 4 (1995) 1-5.

96. Annual Book of ASTM Standards, ASTM E96: Standard Test Methods for Water Vapor Transmission of Materials (1995) 785-792.

97. C. Wang, Y. Li, G. Ding, X. Xie and M. Jiang, "Preparation and characterization of graphene oxide/poly(vinyl alcohol) composite nanofibers via electrospinning", Journal of Applied Polymer Science 127:4 (2012) 3026-3032.

98. F. Khodkar and N. Golshan Ebrahimi, "Preparation and properties of antibacterial, biocompatible core-shell fibers produced by coaxial electrospinning", Journal of Applied Polymer Science 134:25 (2017) 44979.

99. J. Park and S. Kim, "Antimicrobial filtration with electrospun poly(vinyl alcohol) nanofibers containing benzyl triethylammonium chloride: Immersion, leaching, toxicity, and filtration tests", Chemosphere 167 (2017) 469-477.

100. M. Naebe, T. Lin, W. Tian, L. Dai and X. Wang, "Effects of MWNT nanofillers on structures and properties of PVA electrospun nanofibres", Nanotechnology 18:22 (2007) 225605.

101. E. Karimi, A. Raisi and A. Aroujalian, "TiO_2-induced photo-cross-linked electrospun polyvinyl alcohol nanofibers microfiltration membranes", Polymer 99 (2016) 642-653.

102. A. Kozbial, Z. Li, C. Conaway, R. McGinley, S. Dhingra, V. Vahdat, F. Zhou, B. D'Urso, H. Liu and L. Li, "Study on the Surface Energy of Graphene by Contact Angle Measurements", Langmuir 30:28 (2014) 8598-8606.

103. B. Marta, C. Leordean, T. Istvan, I. Botiz and S. Astilean, "Efficient etching-free transfer of high quality, large-area CVD grown graphene onto polyvinyl alcohol films", Applied Surface Science 363 (2016) 613-618.

104. V. Merkle, L. Zeng, M. Slepian and X. Wu, "Core-shell nanofibers: Integrating the bioactivity of gelatin and the mechanical property of polyvinyl alcohol", Biopolymers 101:4 (2014) 336-346.

105. H. Hallaji, A. Keshtkar and M. Moosavian, "A novel electrospun PVA/ZnO nanofiber adsorbent for U(VI), Cu(II) and Ni(II) removal from aqueous solution", Journal of the Taiwan Institute of Chemical Engineers 46 (2015) 109-118.

106. L. Wu, X. Yuan and J. Sheng, "Immobilization of cellulose in nanofibrous PVA membranes by electrospinning", Journal of Membrane Science 250:1-2 (2005) 167-173.

107. J. Li, L. Shao, X. Zhou and Y Wang, "Fabrication of high strength PVA/rGO composite fibers by gel spinning", RSC Advances 4:82 (2014) 43612-43618.

108. M. Muralidharan, S. Mathew, A. Seema, P. Radhakrishnan and T. Kurian, "Optical limiting properties of in situ reduced graphene oxide/polymer nanocomposites", Materials Chemistry and Physics 171 (2016) 367-373.

109. M. Mohd Abdah, N. Zubair, N. Azman and Y. Sulaiman, "Fabrication of PEDOT coated PVA-GO nanofiber for supercapacitor", Materials Chemistry and Physics 192 (2017) 161-169.

110. Y. Jiang, Y. Sun and J. Song, "Fabrication and tribological properties of nanogrids on CVD-grown graphene", Micron 97 (2017) 29-34.

111. S. Surucu and H. Turkoglu Sasmazel, "Development of core-shell coaxially electrospun composite PCL/chitosan scaffolds", International Journal of Biological Macromolecules 92 (2016) 321-328.

112. W. R. Runyan, Semiconductor Measurements and Instrumentation, Texas Instruments Electronic Series, McGraw-Hill, 1965.

113. H. Salavagione, G. Martínez and M. Gómez, "Synthesis of poly(vinyl alcohol)/reduced graphite oxide nanocomposites with improved thermal and electrical properties", Journal of Materials Chemistry 19:28 (2009) 5027-5032.

114. S. Wang, H. Yu and J. Wickliffe, "Limitation of the MTT and XTT assays for measuring cell viability due to superoxide formation induced by nano-scale TiO_2", Toxicology in Vitro 25:8 (2011) 2147-2151.

115. S. Shao, S. Zhou, L. Li, J. Li, C. Luo, J. Wang, X. Li and J. Weng, "Osteoblast function on electrically conductive electrospun PLA/MWCNTs nanofibers", Biomaterials 32:11 (2011) 2821-2833.

116. E. Czekanska, M. Stoddart, R. Richards and J. Hayes, "In search of an osteoblast cell model for in vitro research", European Cells and Materials 24 (2012) 1-17.

117. C. Liu, Z. Xia and J. Czernuszka, "Design and Development of Three-Dimensional Scaffolds for Tissue Engineering", Chemical Engineering Research and Design 85:7 (2007) 1051-1064.